

**Targeted Deletion of the *Ncoa7* Gene Results in Incomplete Distal Renal Tubular Acidosis
in Mice**

Maria Merkulova¹, Teodor G. Păunescu¹, Anil V. Nair¹, Chia-Yu Wang¹, Diane E. Capen¹, Peter
L. Oliver², Sylvie Breton¹ and Dennis Brown¹

¹Program in Membrane Biology, Center for Systems Biology and Division of Nephrology,
Massachusetts General Hospital and Department of Medicine, Harvard Medical School, Boston,
MA

²Department of Physiology, Anatomy and Genetics, University of Oxford, Oxford, UK

Running title: *Ncoa7* knockout mice exhibit incomplete dRTA

Correspondence should be addressed to:

Maria Merkulova, Ph. D.

Program in Membrane Biology and Division of Nephrology

Simches Research Center

185 Cambridge Street, Room 8100

Boston, MA 02114

E-mail: Merkulova.Maria@mgh.harvard.edu

Telephone: (617) 724-0063

Telefax: (617) 643-3182

Abstract:

We recently reported that nuclear receptor coactivator 7 (Ncoa7) is a vacuolar proton pumping ATPase (V-ATPase) interacting protein whose function has not been defined. Ncoa7 is highly expressed in the kidney and partially co-localizes with the V-ATPase in collecting duct intercalated cells (ICs). Here, we hypothesized that targeted deletion of the *Ncoa7* gene could affect V-ATPase activity in ICs *in vivo*. We tested this by analyzing the acid-base status, major electrolytes, and kidney morphology of *Ncoa7* knockout (KO) mice. We found that *Ncoa7* KO mice, similar to *Atp6v1b1* knockouts, did not develop severe dRTA, but they exhibited a persistently high urine pH and developed hypobicarbonatemia after acid loading with ammonium chloride. Conversely, they did not develop significant hyperbicarbonatemia and alkalemia after alkali loading with sodium bicarbonate. We also found that ICs were larger and with more developed apical microvilli in *Ncoa7* KO compared to wild-type mice, a phenotype previously associated with metabolic acidosis. At the molecular level, the abundance of several V-ATPase subunits, carbonic anhydrase 2 and the anion exchanger 1 was significantly reduced in medullary ICs of *Ncoa7* KO mice, suggesting that Ncoa7 is important for maintaining high levels of these proteins in the kidney. We conclude that Ncoa7 is involved in intercalated cell function and urine acidification in mice *in vivo*, likely through modulating the abundance of V-ATPase and other key acid-base regulators in the renal medulla. Consequently, mutations in the *NCOA7* gene may also be involved in dRTA pathogenesis in humans.

Keywords: Ncoa7, dRTA, V-ATPase, knockout mice, intercalated cells

Introduction:

Renal tubular acidosis (RTA) is a group of disorders of various etiologies, in which metabolic acidosis arises from the inability of the renal tubules to secrete protons or reabsorb bicarbonate, while glomerular function is normal (36). Currently three major subgroups of RTA are defined: distal (type 1) RTA, proximal (type 2) RTA and hypoaldosteronism (type 4) RTA, reviewed in (36). The term “type 3 or mixed RTA” originally used to describe a disease with features of both distal and proximal RTA is now obsolete (36). The focus of our current research is on the particular form of distal RTA (dRTA) that is caused by insufficient activity of the kidney collecting duct proton pump, the vacuolar proton pumping ATPase or V-ATPase (also known as H^+ ATPase) (6). V-ATPase is a multisubunit and multi-isoform protein complex that transfers protons across biological membranes, powered by ATP hydrolysis. Kidney-specific V-ATPase is highly expressed in the collecting duct intercalated cells, which are responsible for excretion of protons into the urine (6). This is necessary to maintain systemic acid-base homeostasis at the whole-organism level. Currently, loss-of-function mutations in two V-ATPase genes: *ATP6V1B1* and *ATP6V0A4*, respectively coding for kidney-specific B1 and a4 subunits, have been shown to cause dRTA in humans (1, 20, 41). Insufficient function of the V-ATPase holoenzyme in the absence of these subunits results in acid buildup in the body leading to acidemia and childhood-onset dRTA. If undiagnosed and untreated the disease leads to failure to thrive, growth retardation, osteomalacia or rickets, nephrocalcinosis or nephrolithiasis and eventually kidney failure, and even death in infancy (11). This particular form of dRTA is also characterized by persistently high urine pH, hypobicarbonatemia, hypercalciuria, hypocitraturia and hypokalemia and is accompanied by progressive sensorineural hearing loss (20, 42). It is

caused by mutations in both copies of B1 or a4 V-ATPase subunit genes and is, therefore, inherited in an autosomal recessive manner.

Recently, heterozygous mutations, i.e. mutations in just one copy of either *ATP6V1B1* or *ATP6V0A4* gene, were reported to cause incomplete dRTA (8, 19, 46). Incomplete dRTA is characterized by persistent high urine pH and sometimes hypokalemia and nephrocalcinosis or nephrolithiasis, but acidemia is absent. An acid loading challenge test with ammonium chloride is often used to validate the inability to maximally acidify urine and to confirm a diagnosis of incomplete dRTA (7, 45). Mouse models that resemble both incomplete and complete forms of human dRTA have been developed by targeted deletion of *Atp6v1b1* and *Atp6v0a4* genes respectively (9, 12, 17, 25). *Atp6v0a4* knockout (KO) mice had a severe phenotype with all clinical features of human dRTA (17, 25), while *Atp6v1b1* KO mice were mildly affected and developed metabolic acidosis only after acid loading challenge with ammonium chloride (12). This unexpectedly mild phenotype of *Atp6v1b1* KO mice was proposed to be due to their diet, which produces much less daily acid load than a typical human Western diet (12). The lower acid load could be handled by partial compensation with the homologous B2 isoform of V-ATPase *Atp6v1b2*, which we showed can incorporate into the plasma membrane holoenzyme in B1 null mice (12, 33).

While loss-of-function mutations in *ATP6V1B1* and *ATP6V0A4* genes are very rare and heterogeneous (1), making them difficult to study, next-generation sequencing did identify mutations in these genes in patients with primary dRTA (15, 27). However even this comprehensive approach did not confirm that mutations in suspected V-ATPase-coding genes were present in all of the patients studied (15, 27). In earlier research on another cohort of dRTA patients, no mutations were found in *ATP6V1B1*, *ATP6V0A4* or *ATP6VIC2*, *ATP6VIG3* and

92 *ATP6V0D2*, three other genes coding for the remaining kidney-specific subunits of V-ATPase
93 (40). These data suggest that in some patients, mutations in genes other than those coding for the
94 recognized core subunits of V-ATPase can reduce V-ATPase function and cause hereditary
95 forms of dRTA. It is possible that these other genes code for proteins that are not structural
96 components of the pump, but rather interact with V-ATPase to modulate its function. Very
97 recently, for example, three patients with recessive mutations in the V-ATPase transcription
98 regulator FoxI1 were reported to have acidosis and sensorineural deafness (10).

99 We recently performed the first systematic proteome-wide analysis of V-ATPase protein-
100 protein interactions in kidney and discovered several novel V-ATPase interacting proteins (24).
101 One of the highest scoring interacting proteins was Ncoa7 (for nuclear receptor coactivator 7),
102 whose *in vivo* function is unknown. Human NCOA7 was originally discovered as an estrogen
103 receptor binding protein more than 20 years ago (16), and subsequently it was shown to bind
104 other nuclear receptors as well (39). However, its role in the signaling properties of these
105 receptors *in vivo* is still not understood. More recently, NCOA7 has been classified as a member
106 of a small group of so-called TLDC (for TBC and LysM domain containing) antioxidant proteins
107 and its role in protection from oxidative stress *in vitro* has been confirmed, although the
108 mechanism remains unknown (13). In humans and mice there are four other TLDC domain-
109 containing proteins: OXR1, which is in addition a NCOA7 homologue, and TBC1D24, TLDC1
110 and TLDC2, differentially expressed in different tissues. (13). In particular, Ncoa7 is expressed
111 at higher levels in certain tissues and organs, including kidney (13, 35, 39). In agreement with
112 these reports, we found that Ncoa7 was co-expressed and partially co-localized with V-ATPase
113 in the apical pole of kidney collecting duct intercalated cells, as such, it may play a specific role
114 in V-ATPase regulation in these cells (24).

Here, we hypothesized that loss-of-function mutations in the *Ncoa7* gene could affect V-ATPase activity in kidneys *in vivo*, possibly causing dRTA. To test this hypothesis, we took advantage of *Ncoa7* KO mice that had been generated as part of the Knockout Mouse Project KOMP2-DTCC (5, 21). We analyzed their acid-base status, major electrolytes and kidney morphology in comparison with wild-type (WT) mice as well as prior data from *Atp6v1b1* and *Atp6v0a4* KO mice. We found that unlike *Atp6v0a4* KO mice, *Ncoa7* knockouts did not develop severe dRTA. However, they had a persistently high urine pH and demonstrated hypobicarbonatemia after acid loading with ammonium chloride. Therefore, they most closely resemble the incomplete dRTA phenotype of *Atp6v1b1* KO mice. After alkali loading with sodium bicarbonate *Ncoa7* knockouts did not develop significant hyperbicarbonatemia and alkalemia, consistently with the mild acidotic state of these animals. We also found that morphologically, intercalated cells were larger and sometimes formed continuous rows of adjacent cells in *Ncoa7* KO compared to WT mice, a phenotype previously associated with metabolic acidosis (22). Finally, levels of several V-ATPase subunits, carbonic anhydrase 2 and anion exchanger 1 were significantly reduced in the kidney medulla of the *Ncoa7* KO mice.

Materials and Methods:

Mice

The *Ncoa7* knockout mouse line C57BL/6N-*Ncoa7*^{tm1.1(KOMP)Vlcr}/Tcp was generated as part of the Knockout Mouse Project KOMP2-DTCC (<https://www.komp.org/>) with C57BL/6N-*Ncoa7*^{tm1(KOMP)Vlcr}/Tcp made from KOMP ES cells (5) at the Toronto Centre for Phenogenomics (Toronto, ON, Canada). More specifically, the parental tm1 mouse line

138 C57BL/6N-*Ncoa7*<tm1(KOMP)Vlcr>/Tcr was created by the insertion of the Velocigene
139 cassette ZEN-Ub1 containing a LacZ (β -galactosidase) coding sequence and a LoxP-flanked
140 neomycin-resistance gene (Fig. 1A). This insertion resulted in a deletion of size 49126bp in the
141 *Ncoa7* gene locus spanning exons 2 and 3 and the intronic sequence between them. Next,
142 breeding of a heterozygous C57BL/6N-*Ncoa7*<tm1(KOMP)Vlcr>/Tcr male with heterozygous
143 C57BL/6N-Gt(ROSA)26Sor<tm1(ACTB-Cre,-EGFP)Ics>/Tcr females resulted in Cre excision
144 of the neomycin-resistance gene leaving behind the inserted *lacZ* reporter sequence, which is
145 now under the regulation of the native *Ncoa7* promoter (Fig. 1A). The mouse tm1.1 line
146 C57BL/6N-*Ncoa7*<tm1.1(KOMP)Vlcr>/Tcr (hereafter referred to as *Ncoa7* KO) was then
147 established by backcrossing *Ncoa7*<tm1.1+/->; Cre<-> mice to C57BL/6NCrl. These mice were
148 obtained from the Canadian Mouse Mutant Repository (Toronto, ON, Canada) as heterozygous
149 animals. Mice were then bred in-house to generate homozygotes. For genotyping, genomic DNA
150 was extracted from mouse tails using the KAPA Express Extract Kit (Kapa Biosystems,
151 Wilmington, MA). Genotyping was performed by PCR using the KAPA Mouse Genotyping Kit
152 (Kapa Biosystems) and the following primer pairs: 1) F1 5'-
153 TTTGAAGAATGGCTGCTCCGTGTGGG-3' and R1 5'-
154 ATGCAGCAGAAACGTGGCCAAGAGAC-3' to detect a wild-type allele or 2) F2 5'-
155 CCATTACCAGTTGGTCTGGTGTC-3' and R2 5'-
156 TTTGAGACAGGGCCTTAGTAACCTGGGC-3' to detect a mutant allele.

157 To confirm that *Ncoa7* full-length mRNA transcripts were absent from KO mice, end-
158 point RT-PCR was carried out as briefly described. Total kidney RNA was isolated using
159 RNeasy Mini Kit (Qiagen, Germantown, MD) according to the manufacturer's protocol. First-
160 strand cDNA was then synthesized from 1 μ g RNA using the High-Capacity cDNA Reverse

Transcription Kit (Applied Biosystems, Foster City, CA). PCR reactions were performed using the PowerUp SYBR Green Master Mix on a QuantStudio3 Real-Time PCR system (Applied Biosystems). The *Ncoa7* exon 3-specific primers F3 5'-CAGCTGCGTCCTCGAAGAG-3' and R3 5'-GCTGTAAACGTTGAACTTGTCTTGTTC-3' were used to detect *Ncoa7* full-length transcripts; while *Rpl19* (ribosomal protein L19)-specific primers 5'-CCCGTCAGCAGATCAGGAA-3' and 5'-GTCACAGGCTTGCGGATGA-3' were used to amplify *Rpl19* cDNA as a loading control. To confirm that *Ncoa7* protein is absent from KO mice, an affinity-purified rabbit polyclonal antibody raised against the 1-350 a.a. fragment of *Ncoa7* (23092-1-AP, Proteintech, Chicago, IL) was used for western blotting using lysates from WT and *Ncoa7* KO kidneys as described below.

For all experiments, control mice (referred to as WT) were either littermates or age-matched C57BL/6NCrl mice (Charles River Laboratories, Wilmington, MA) as indicated. The experimental unit is always a single mouse. All animal studies were approved by the Massachusetts General Hospital Subcommittee on Research Animal Care, in accordance with the NIH, Department of Agriculture, and Association for the Assessment and Accreditation of Laboratory Animal Care requirements.

Blood and urine analysis

In control experiments WT and *Ncoa7* KO 4-5 month old mice were maintained on a standard rodent diet (Prolab® Isopro® RMH 3000, LabDiet, St. Louis, MO) with free access to water. For acid loading challenge, drinking water was substituted with 0.28 M NH₄Cl/1% sucrose for 3 days (12, 33). For alkali loading challenge, drinking water was substituted with 0.28 M NaHCO₃/1% sucrose for 3 days (4). 1% sucrose was added to both acidified and

184 alkalized water to ensure, that mice drank normally and remained hydrated. In preliminary
185 experiments we found that treatment with 1% sucrose vs. plain water did not have any significant
186 effect on acid-base status; sodium, potassium and chloride levels, as well as urine osmolality in
187 either WT or *Ncoa7* KO mice (data not shown). In addition, mice of both genotypes drank the
188 same amount of sweetened as plain water (data not shown). Thus, for standard diet experiments
189 mice were provided plain water, as in previous studies on acid-loading (4, 12).

190 For measurement of blood gases and pH, whole blood was collected from the
191 submandibular vein of conscious mice. It was immediately tested with a Radiometer ABL800
192 FLEX analyzer (Radiometer, Copenhagen, Denmark). Blood bicarbonate concentration was
193 calculated from the measured pH and pCO₂ values using the Henderson-Hasselbalch equation.
194 For sodium, potassium and chloride measurements mice were terminally anesthetized with
195 sodium pentobarbital (Nembutal, Abbott Laboratories, Abbott Park, IL, 50 mg/kg body weight,
196 intraperitoneally) and blood was collected from the open heart. Serum was then separated using
197 BD Microtainer SST serum collection tubes (Becton, Dickinson and Co., Franklin Lakes, NJ).
198 Serum electrolytes (sodium, potassium and chloride) were measured at the Massachusetts
199 General Hospital Veterinary Clinical Pathology Core Facility using a Heska Dri-Chem 7000
200 analyzer (Heska, Loveland, CO). The hemolyzed serum samples, as assessed based on their color
201 were excluded from the final potassium level analysis. For spot urine pH measurement, mouse
202 urine was collected directly onto Hydrion Urine & Saliva pH Paper 5.5-8.0 (Micro Essential
203 Laboratory Inc., Brooklyn, NY) or colorpHast pH 7.5-14.0 strips (EMD Millipore, Burlington,
204 MA) and pH was read immediately by two different, blinded investigators. For measuring spot
205 urine osmolality, urine drops were first collected on Parafilm and then immediately placed into

capped microtubes to minimize evaporation. Urine osmolality was measured the same day using a Vapro 5600 vapor pressure osmometer (Wescor, Logan, UT).

Blood pressure measurement.

Blood pressure was measured in WT (n = 14) and *Ncoa7* KO (n = 12) 4-5 month old mice by tail-cuff manometry using a CODA non-invasive monitor (Kent Scientific, Torrington, CT). One or two days prior to the actual measurements mice were trained to be restrained in a plastic tube holder (Kent Scientific) with occlusion and volume-pressure recording (VPR) cuffs placed over their tails. On the day of the experiment each mouse was again first adapted to the holder for 5 minutes prior to the blood pressure measurement. Mice were always warmed by heating pads to maintain proper blood circulation in their tails. All measurements were taken in the late morning (10 am - 12 pm) and values from approximately 10 measurement cycles per mouse were averaged.

Semi-quantitative western blotting and co-immunoprecipitation.

4-5 month old mice were terminally anesthetized with sodium pentobarbital (Nembutal, Abbott Laboratories, Chicago, IL, 50 mg/kg body weight, intraperitoneally). Kidneys were dissected, transverse sections were cut with a razor blade, cortex was separated from medulla, and both regions were either lysed immediately or snap frozen in liquid nitrogen for storage at –80°C. Lysis was done in ice-cold RIPA buffer (50 mM Tris-HCl, 150 mM NaCl, 1% NP-40, 0.5% sodium deoxycholate, and 0.1% SDS, pH 7.4; Boston BioProducts, Ashland, MA), containing Complete Protease Inhibitor cocktail (Roche Applied Science, Indianapolis, IN) and clarified by centrifugation at 16,000 g. Total protein concentration was determined using a Pierce

BCA Protein Assay Kit (Thermo Fisher Scientific, Waltham, MA). An equal amount (7.5 μ g) of each protein sample was loaded on Novex NuPAGE 4-12% Bis-Tris gels (Thermo Fisher Scientific). Protein separation and transfer to PVDF membrane (Thermo Fisher Scientific) was performed as previously described (44). Equal loading and transfer to the membrane was further confirmed by Ponceau S staining (Sigma-Aldrich, St. Louis, MO). Western blotting was performed as described elsewhere (44). The following primary antibodies were used: affinity-purified rabbit polyclonal anti-V-ATPase B1 (30), B2 (28), A (18) and a4 (18) subunit antibodies, an affinity-purified rabbit polyclonal anti-Ncoa7 1-350 a.a. (0.36 μ g/ml, 23092-1-AP, Proteintech), a sheep polyclonal raised against carbonic anhydrase II (14.6 μ g/ml, IgG fraction, ab8953, Abcam, Cambridge, MA) and an affinity-purified anti-AE1 (anion exchanger 1, a.k.a. Slc4a1) rabbit polyclonal antibody (2) kindly provided by Dr. Seth Alper (Beth Israel Deaconess Medical Center, Boston, MA). The developed films were scanned and digital images were analyzed and quantified using ImageJ software (version 1.51(100), National Institutes of Health, Bethesda, MD) (38). Co-immunoprecipitation of Ncoa7 and the B1-V-ATPase subunit was performed as described previously (24).

Immunohistochemistry and fluorescence microscopy:

Fixation of WT and *Ncoa7* KO 5-month old mouse kidneys, preparation and storage of cryostat sections, rehydration, antigen retrieval, and incubation with primary and secondary antibodies were performed as previously described (24, 44). In each experiment kidney sections from WT and *Ncoa7* KO mice were processed and incubated in parallel, using at least 4 mice per genotype. The affinity-purified rabbit polyclonal anti-V-ATPase B1 subunit antibody (30) was used at 1:400. The secondary Alexa 488-conjugated goat anti-rabbit IgG antibody (Molecular

Probes/Thermo Fisher Scientific, Waltham, MA) was used at 5 μ g/ml. For double immunostaining, we used concurrently an affinity-purified anti-AE1 at 1:600 and an affinity-purified chicken polyclonal anti-V-ATPase A subunit antibody (24) at 1:200; or an affinity-purified rabbit polyclonal anti-V-ATPase A subunit antibody (18) at 1:200 and an affinity-purified chicken polyclonal anti-V-ATPase B2 subunit antibody (29) at 1:400. The secondary indocarbocyanine Cy3-conjugated donkey anti-rabbit IgG and Alexa 488-conjugated donkey anti-chicken IgY antibodies (both from Jackson ImmunoResearch, West Grove, PA) were used at 1.9 μ g/ml and 15 μ g/ml, respectively. Immunostained kidneys were imaged with a Nikon 80i epifluorescence microscope (Nikon Instruments, Melville, NY) using an Orca 100 CCD camera (Hamamatsu, Bridgewater, NJ). Alternatively, digital images were acquired using an LSM 800 confocal laser scanning microscope (Carl Zeiss Microscopy, Thornwood, NY), controlled by ZEN 2 (blue edition) software (Carl Zeiss Microscopy). For comparative semi-quantitative analysis confocal images of WT and *Ncoa7* KO kidneys were acquired under identical conditions, including the same exposure time and other imaging parameters. Images were post-processed using Adobe Photoshop CS4 image-editing software (Adobe Systems, San Jose, CA). Representative images from a total of 8 mice per genotype are shown.

Transmission and immunogold electron microscopy:

Conventional transmission and immunogold electron microscopy were performed on 5-month old mouse kidney medullas (n=4 mice per genotype) as described elsewhere (31, 32). Briefly, for conventional transmission electron microscopy (TEM), following perfusion/immersion fixation with periodate-lysine-paraformaldehyde (PLP) reagent, small pieces of WT and *Ncoa7* KO kidney medullas were immersed in 2.0% glutaraldehyde in 0.1 M

275 sodium cacodylate buffer, pH 7.4. They were post-fixed for 1 h in 2% osmium tetroxide,
276 dehydrated through a graded series of ethanol solutions up to 100% and embedded in Epon
277 (Electron Microscopy Sciences, Fort Washington, PA). Thin (~70 nm) sections were collected
278 onto copper slot grids and stained with uranyl acetate and Reynold's lead citrate prior to
279 examination. Sections were examined in a JEM-1011 transmission electron microscope (JEOL
280 Ltd., Tokyo, Japan) at 80 kV.

281 For immunogold staining, following perfusion/immersion fixation with PLP, kidney
282 medulla tissue was dehydrated as described above, and embedded and polymerized in LR White
283 resin (Electron Microscopy Sciences) at 50 °C. Thin (~70 nm) sections were collected onto
284 nickel slot grids and incubated on drops of primary rabbit anti-V-ATPase (B1-subunit, 1:100)
285 antibody (30) for 1-2 h. After rinsing with PBS, the grids were incubated on drops of goat anti-
286 rabbit IgG antibody coupled to 15 nm gold particles (Ted Pella, Redding, CA) for 1 h. Following
287 several rinses with distilled water, the grids were stained with 2% uranyl acetate for 5 min, rinsed
288 again in distilled water, dried and examined as described above for TEM.

289

290 Quantification of number and size of intercalated cells.

291 Intercalated cells (ICs) were identified based on their V-ATPase immunostaining in
292 digital epifluorescence images acquired as described above, and were counted manually (44) in
293 the entire inner stripe (IS) of the outer medullary region, whose area was measured on mid-
294 transverse kidney sections using freehand selections in ImageJ software. We performed these
295 measurements in sections from 4 WT and 4 *Ncoa7* KO mice, containing on average 544 ICs per
296 4.8 mm² of IS area per animal. To calculate IC density in the IS, the manually counted number of
297 IC was divided by the area of the entire IS region. A similar measurement was performed for the

IC-containing upper region of the inner medulla (IM); an average of 258 IM ICs in the proximal 2 mm² IM area per animal from 4 WT and 4 *Ncoa7* KO mice were counted.

Size of the ICs identified based on their morphology was assessed by measuring total cell area in TEM images acquired as described above, using freehand selections in ImageJ software as previously described (31). We performed these measurements in a blinded manner on an average of 50 IS ICs per genotype from 3 WT and 5 *Ncoa7* KO mice.

Statistics

Statistical significance was determined by two-tailed unpaired t-test using Prism 7 software (GraphPad Software, La Jolla, CA). $P < 0.05$ was considered significant. Graphs were plotted with Prism 7 software. Experimental values are reported as means \pm standard error of the mean (SEM).

Results

Ncoa7 KO mice have an overall normal phenotype and blood pH, but high urine pH when fed a standard rodent diet.

Ncoa7 KO mice were generated as part of the Knockout Mouse Project KOMP2-DTCC (5, 21) as described in more detail in Materials and Methods. The gene targeting strategy resulting in deletion of *Ncoa7* coding exons 2 and 3 and simultaneous incorporation of a *lacZ* reporter is shown in Fig. 1A. Mice were obtained as heterozygotes and then bred in-house to generate homozygous mice. Offspring genotyping was performed by PCR on tail genomic DNA using primer pairs F1/R1 and F2/R2, specific for the wild-type and mutant alleles respectively, confirming successful gene targeting (Fig. 1B). Wild-type, heterozygous and homozygous mice were born at normal Mendelian 1:2:1 ratios. Absence of full-length *Ncoa7* transcripts in homozygous *Ncoa7* KO mice was demonstrated by end-point RT-PCR using total kidney RNA and an exon 3-specific primer pair F3/R3 (Fig. 1C). By Western blotting we confirmed that the full-length protein of ~140 kDa, detected by polyclonal antibodies raised against 1-350 N-terminal a.a. of *Ncoa7*, is absent in kidneys of *Ncoa7* KO mice (Fig 1D). The lower molecular weight protein bands that are also detected by these antibodies are mostly absent in *Ncoa7* KO mice. These lower molecular weight proteins could be a result of *Ncoa7* degradation, and they do not interact with the B1 subunit V-ATPase in immunoprecipitation studies (Fig. 1E). By immunofluorescence microscopy using these same antibodies, we clearly detected *Ncoa7* in WT kidney intercalated cells, identified by co-staining for V-ATPase (Fig. 1F), but not in *Ncoa7* KO mice (Fig. 1G).

Homozygous *Ncoa7* KO mice were viable and fertile, with normal weight and without gross anatomical or physiological abnormalities, when maintained under standard rodent

husbandry and dietary conditions. Our observations are consistent with the data obtained during systematic broad-based standardized phenotyping of *Ncoa7* KO mice performed by the International Mouse Phenotyping Consortium (IMPC, <http://www.mousephenotype.org/>). However, IMPC did not measure the blood pressure of *Ncoa7* KO mice. We found that the average systolic blood pressure of *Ncoa7* KO mice was 89.8 ± 3.2 mmHg (mean \pm standard error of the mean, SEM, $n=12$) vs 103.0 ± 1.7 mmHg ($n=14$) in WT controls, $p = 0.0008$. Besides lower blood pressure, *Ncoa7* KO mice had an overall normal phenotype, suggesting that there is no severe systemic acid-base imbalance in these mice. Indeed, there was no significant difference between WT and KO mice in blood pH (7.26 ± 0.02 vs. 7.26 ± 0.02 respectively; Fig. 2a and Table 1, standard diet) and serum HCO_3^- level (20.31 ± 0.84 vs. 20.43 ± 0.81 mM; Fig. 2b and Table 1, standard diet). In addition, there were no significant differences in serum sodium, potassium and chloride levels (Table 1, standard diet). However urine pH was significantly higher in KO than in WT mice (6.98 ± 0.13 vs. 6.15 ± 0.08 , respectively, $p < 0.0001$; Fig. 2c and Table 1, standard diet), suggesting an inability to maximally acidify urine, which points to incomplete dRTA. These results indicate that *Ncoa7* is involved in urine acidification *in vivo* in mice. However, it is not absolutely required to maintain normal blood pH in mice fed a standard rodent diet.

Ncoa7 KO mice develop hypobicarbonatemia without acidemia after acid loading with ammonium chloride.

To confirm the diagnosis of incomplete dRTA, *Ncoa7* KO and WT mice were challenged by acid loading *ad libitum* with 0.28 M ammonium chloride administration in their drinking water for 3 days. Both *Ncoa7* KO and WT mice drank the same amount of acidified water, compared to plain water, with no significant difference between genotypes (Table 1), and the

ammonium chloride loading was very similar in mice of both genotypes (0.046 ± 0.003 vs 0.042 ± 0.003 mmol/g body weight in WT and *Ncoa7* KO mice respectively, Table 1). This acid load was not sufficient to lower blood pH either in WT or in KO animals (7.23 ± 0.03 and 7.22 ± 0.04 respectively; Fig. 2a and Table 1, acid load). In contrast, HCO_3^- levels were significantly reduced in *Ncoa7* KO mice (14.71 ± 1.31 vs. 20.43 ± 0.81 mM, $p = 0.001$; Fig. 2b and Table 1, -/- acid load vs. standard diet). A trend towards lower HCO_3^- levels upon acid loading was also observed in WT mice but it did not reach statistical significance (17.58 ± 1.17 vs. 20.31 ± 0.84 ; $p = 0.0678$; Fig. 2b and Table 1, +/+ acid load vs. standard diet). These results suggest that *Ncoa7* KO mice are more susceptible to acidotic stress than WT controls. After treatment with ammonium chloride, pCO_2 levels were also significantly lower in *Ncoa7* KO than in WT mice (36.46 ± 2.17 vs. 43.43 ± 2.14 mmHg, $p = 0.0384$; Table 1, acid load). This decrease was also statistically significant when comparing untreated to acidified *Ncoa7* KO mice (46.52 ± 0.60 vs. 36.46 ± 2.17 mmHg, $p < 0.0001$; Table 1, -/- standard diet vs. acid load), but not when untreated and acidified WT mice are compared (46.24 ± 1.31 vs. 43.43 ± 2.14 mmHg; Table 1, +/+ standard diet vs. acid load). The pCO_2 results suggest that blood pH remained similar in WT and *Ncoa7* KO mice despite significantly reduced bicarbonate levels in KO mice apparently due to loss of CO_2 via respiratory compensation for NH_4Cl -induced acidosis.

Next, major electrolytes were measured in serum from both WT and *Ncoa7* KO mice, acidified with ammonium chloride and compared to untreated animals. Upon acidification, chloride and sodium levels increased and to a similar degree in both WT and *Ncoa7* KO mice with no significant difference between genotypes (Table 1). There was no statistically significant difference in potassium levels between genotypes on either diet or when comparing each genotype on standard or acidified diet (Table 1). Finally, urine pH was strongly reduced after

NH₄Cl treatment in both WT and KO mice, but was still significantly higher in KO mice (5.86 ± 0.04 in KO vs. 5.57 ± 0.03 in WT, $p < 0.0001$; Fig. 2c and Table 1, acid load). Thus, *Ncoa7* KO mice were unable to maximally acidify their urine after acid loading with ammonium chloride, demonstrating incomplete dRTA.

Ncoa7 KO mice do not develop significant hyperbicarbonatemia and alkalemia after alkali loading with sodium bicarbonate.

To further characterize the acid-base status of *Ncoa7* mice, we challenged them with an alkali load *ad libitum* by 0.28 M sodium bicarbonate administration in their drinking water for 3 days. In contrast to acid loading, both WT and *Ncoa7* KO mice drank significantly more medicated than plain water; therefore, their alkali load was greater than the acid load and was not significantly different between genotypes (0.100 ± 0.019 vs 0.093 ± 0.008 mmoles/g body weight in WT and *Ncoa7* KO mice respectively, Table 2). This amount of alkali load was sufficient to induce a significant increase of blood pH (7.38 ± 0.01 vs 7.26 ± 0.02 , $p = 0.0084$; Fig. 2a and Table 2, +/- alkali load vs. standard diet) and blood bicarbonate (25.78 ± 0.93 vs. 20.31 ± 0.84 mM, $p = 0.0033$; Fig. 2b and Table 2, +/- alkali load vs. standard diet) in WT mice, but not in *Ncoa7* KO mice (Fig. 2b and Table 2). The absence of significant hyperbicarbonatemia and alkalemia after alkali loading in *Ncoa7* KO mice further confirms that acid-base balance in these mice is slightly shifted towards acidosis. Surprisingly, in spite of changes in blood pH, both WT and *Ncoa7* KO mice tolerated alkali loading well, and we did not observe any apparent health issues. We also found, that sodium, potassium and chloride levels in serum were not significantly different in either WT or *Ncoa7* KO mice drinking either plain or alkalized water (Table 2). Finally, urine pH was strongly increased after NaHCO₃ treatment in

both WT and KO mice, but was still significantly higher in KO mice (8.5 ± 0.2 in KO vs. 7.15 ± 0.04 in WT, $p = 0.0199$; Fig. 2c and Table 2, alkali load).

V-ATPase subunits, carbonic anhydrase 2 and the anion exchanger 1 are downregulated in the kidney medulla of *Ncoa7* KO mice.

To study the mechanisms underlying the observed urinary acidification defects in *Ncoa7* KO mice we analyzed the abundance of several subunits of V-ATPase in the kidneys of these mice by Western blotting. We found that compared to WT controls, levels of kidney specific B1 and a4 subunits of V-ATPase were decreased by more than 80% and levels of the ubiquitous B2 and A subunits were decreased by more than 60% (Fig. 3). We also found that levels of carbonic anhydrase 2, Car2 (a.k.a. Ca2) and the anion exchanger 1, AE1 (a.k.a. Slc4a1) are downregulated by approximately 60% and 40% respectively in *Ncoa7* KO compared to WT mice (Fig. 3). Thus, two other key proteins involved in regulation of acid-base homeostasis by kidney are downregulated in *Ncoa7* KO mice.

To visualize downregulation of V-ATPase levels *in situ* we performed confocal immunofluorescence imaging with antibodies against the A and B2 subunits of V-ATPase. We found that in *Ncoa7* KO mice levels of both A and B2 subunits are downregulated in intercalated cells from the inner stripe of the outer medulla (Fig. 4). The outer medulla is the major site of “distal” proton secretion in the kidney (23), and we suggest that downregulation of V-ATPase levels in this region underlines the impaired urinary acidification seen in *Ncoa7* KO mice.

Ncoa7 KO mice may adapt to systemic acidemia by upregulation of size and activity, but not the number of intercalated cells.

427 To address the question whether *Ncoa7* deletion, followed by V-ATPase downregulation
428 has other effects on cellular and subcellular morphology of the kidney, renal tissue from *Ncoa7*
429 KO mice was further examined by fluorescence and electron microscopy. First, kidney ICs were
430 visualized by immunofluorescence using antibodies against the IC-specific B1 subunit of V-
431 ATPase, and AE1 to distinguish A and B type intercalated cells. Cells double-positive for B1 and
432 AE1 are A type ICs, while cells positive for B1 only are B type ICs. We then analyzed A type
433 ICs, referring to them as ICs (2). We found continuous rows of adjacent ICs in outer medullary
434 collecting ducts in *Ncoa7* KO mice, particularly in the inner stripe (IS) of the outer medulla,
435 while in WT mice only individual, isolated ICs were found in this region, as is usually the case
436 (Fig. 5). While the presence of continuous rows of adjacent ICs in *Ncoa7* KO mice gave the
437 impression that there is an increased number of ICs in kidneys of these mice, a subsequent
438 quantification of ICs in the entire IS (113.9 ± 10.5 cells/mm² in WT vs. 118.4 ± 11.0 cells/mm²
439 in KO, $p = 0.7772$; Fig. 6a) and the proximal 2 mm² of the inner medulla (147.4 ± 23.2
440 cells/mm² in WT vs. 126.6 ± 19.1 cells/mm² in KO, $p = 0.5134$; Fig. 6b) did not reveal a
441 significant difference in their number between genotypes. Next, we noted that *Ncoa7* KO ICs are
442 larger than ICs from WT mice (Fig. 5). To quantify the size difference of ICs of *Ncoa7* KO mice
443 compared to WT mice, we examined them by transmission electron microscopy. We also
444 compared ultrastructural morphological details between ICs from KO and WT mice using TEM.
445 This technique allowed us to easily distinguish ICs based on their morphology, because they
446 have an electron-dense cytoplasm with numerous mitochondria, tubulovesicles, and microvilli
447 (3). Side-by-side comparison of electron micrographs of ICs from WT and *Ncoa7* KO mice
448 again revealed that ICs were larger in *Ncoa7* KO mice, and at least two adjacent intercalated
449 cells could be found frequently in *Ncoa7* KO (Fig. 7 B and D), but not in WT mice (Fig. 7 A and

C). In addition, apical microvilli were more developed (i.e., longer and more numerous) in ICs from *Ncoa7* KO mice compared to their WT counterparts (Fig. 7), indicating a more activated state of these cells in KO mice (31). Frequently, small slivers of principal cell cytoplasm were seen between the overgrown ICs and sometimes just very thin cell projections were captured on the tissue sections (Fig. 7B, arrows). By immunogold electron microscopy we observed that V-ATPase accumulates in the apical microvilli of kidney ICs in *Ncoa7* KO mice (Fig. 8). Finally, quantification of IC area in electron microscopy images of kidney sections revealed that area of IC in *Ncoa7* KO is on average 40% larger than of IC in WT mice (93.87 ± 4.92 vs. 66.28 ± 2.83 μm^2 , respectively, $p < 0.0001$; Fig. 9). In summary, in kidneys of *Ncoa7* KO mice, the size but not number of ICs was increased and V-ATPase was present at the apical plasma membrane of these cells. Functionally these morphological changes should lead to an increase in V-ATPase-driven proton excretion into the urine, lowering its pH. However, because of the lower protein abundance of V-ATPase in kidney medulla of *Ncoa7* KO mice, they still produce urine with higher than normal pH, although various compensatory mechanisms were present that partially prevented a major acid-base phenotype in these animals.

Discussion:

In this study we found that *Ncoa7* KO mice demonstrate features of incomplete dRTA and can serve as a novel model of this disease. When comparing *Ncoa7* KO mice to *Atp6v1b1* and *Atp6v0a4* KO animals with V-ATPase deficiencies, *Ncoa7* KO do not develop a severe metabolic acidosis, as seen in *Atp6v0a4* knockouts (17, 25), but have a phenotype that more closely resembles that of B1 KO animals (12). Both *Ncoa7* and *Atp6v1b1* KO mice (12) produce urine with persistently high pH, which remains inappropriately high even after acid loading with ammonium chloride. After ammonium chloride treatment, both *Ncoa7* and *Atp6v1b1* KO mice (12) develop hypobicarbonatemia. However, while acidified *Atp6v1b1* KO mice also develop acidemia (12), *Ncoa7* KO mice did not. Preservation of the relatively normal blood pH in acidified *Ncoa7* KO mice in comparison with acidified *Atp6v1b1* KO mice can be explained in part by the fact that respiratory compensation was apparently sufficient to maintain normal systemic pH in *Ncoa7* but not in *Atp6v1b1* KO mice. We also found that compensatory processes involve morphological remodeling of collecting ducts in kidneys of *Ncoa7* KO mice. In particular, we detected an increase in size of ICs, as well as an amplification of their apical microvilli. The latter feature has been associated with increased proton secretion in various studies (31, 34, 37). Metabolic and respiratory acidosis are known to cause such adaptive morphological changes (22), and this confirms that *Ncoa7* KO mice are under some degree of acidotic stress. Interestingly, we have previously observed similar remodeling of kidney collecting ducts in rats treated with the carbonic anhydrase inhibitor, acetazolamide, which is known to induce metabolic acidosis (3). The mild phenotype of *Ncoa7* mice is somewhat expected because if as we hypothesize, *Ncoa7*'s major function is in the modulation of V-ATPase abundance and activity, *Ncoa7* deletion should have a less severe impact on V-ATPase

than the complete absence of V-ATPase structural components, such as a core catalytic subunit in *Atp6v1b1* KO mice. Finally, we found that *Ncoa7* deletion was somewhat protective against alkali loading, because in contrast to WT mice *Ncoa7* KO mice did not develop significant hyperbicarbonatemia and alkalemia after alkali loading with sodium bicarbonate.

Mutations in the *NCOA7* gene can possibly be implicated in dRTA pathogenesis in humans as well. As is the case with *ATP6V1B1*, an *NCOA7* loss-of-function phenotype may be more severe in humans than in mice and may result in complete dRTA with acidemia (20). We suggest that patients with dRTA, especially if accompanied by progressive hearing loss, could be screened for mutations in the *NCOA7* gene if mutations in V-ATPase core genes are not found. As mentioned above, *Ncoa7* is one of many proteins that we found in our screen to interact with V-ATPase in kidney. In fact, its “interaction score” was actually greater than for some of the “core” subunits of the V-ATPase, implying that it has an intimate and important role in V-ATPase function (24). Here we found that the abundance of several subunits of V-ATPase, in particular B1, B2, A and a4 is greatly decreased in kidney medullary ICs of *Ncoa7* KO mice, suggesting that *Ncoa7* is important for maintaining high levels of V-ATPase in these cells. Interestingly, we found that the abundance of carbonic anhydrase 2 and anion exchanger 1 is also decreased in kidney medulla of *Ncoa7* KO mice, suggesting that expression of three key components, involved in the regulation of acid-base homeostasis by kidney - V-ATPase, Car2 and AE1 - is coordinated. The simultaneous decrease in the expression of all three proteins leads to the mild acidosis defect observed in *Ncoa7* KO mice.

Downregulation of E and a4 subunits of V-ATPase in the kidneys of *Atp6v1b1* KO mice has been previously reported by our group, suggesting that levels of some V-ATPase subunits may also be tightly coordinated (44). In addition, levels of A, E, and H subunits were decreased

in a pure population of ICs, isolated by fluorescence-activated cell sorting (FACS) from hybrid EGFP-expressing *Atp6v1b1* KO mice; in contrast, the B2 subunit of V-ATPase was upregulated in this pure population of ICs (44). The mechanism for this coordinated downregulation of some V-ATPase subunits and upregulation of the others, has not been determined, but it was proposed that individual V-ATPase subunits may have a diminished stability outside of the fully assembled complex (44). In this study we did not analyze pure FACS-sorted populations of ICs, but by *in situ* imaging we found that levels of both A and B2 subunits are downregulated in ICs of *Ncoa7* KO mice, despite their apparently “activated” phenotype. We also did not observe relocation of the V-ATPase B2 subunit to the apical pole of *Ncoa7* KO ICs, which occurs in *Atp6v1b1* KO mice as a compensatory mechanism for B1 subunit loss of function in kidneys (33). Thus, our data suggest that upregulation of B2 levels and its relocation to the apical pole of ICs occurs only in the complete absence of the B1 subunit of V-ATPase, such as in *Atp6v1b1* KO mice, but not when B1 levels is still present, even at reduced levels in the *Ncoa7* KO mice.

By analogy with the B2 compensatory mechanism, the *Ncoa7* homologue, *Oxr1* (for oxidation resistance 1) which was also found in our V-ATPase interactome screen (24) may compensate, at least partially, for *Ncoa7* function in the kidney. Deletion of *Oxr1* in mice results in cerebellar neurodegeneration and ataxia, as well as postnatal growth retardation and premature death (26). In contrast to *Oxr1* KO mice we did not observe any overt neurological defects, such as ataxia, in *Ncoa7* KO mice. Potential renal abnormalities have not yet been examined in *Oxr1* KO mice. We suggest, therefore, that the renal phenotype should be thoroughly evaluated in *Oxr1* KO mice also.

In conclusion, our results show that *Ncoa7* is involved in urine acidification *in vivo* in mice, apparently through modulation of V-ATPase, as well as *Car2* and *AE1* levels in the kidney

medulla. The precise mechanism of this modulation is currently unknown, but we suggest that it occurs at the protein level initially through the V-ATPase, based on our previous finding that Ncoa7 physically interacts with the B1 subunit of V-ATPase (24). Since V-ATPase is a multisubunit membrane-bound protein complex, we hypothesize that Ncoa7 may be directly involved in the stabilization or trafficking of V-ATPase individual subunits (such as B1), partially assembled sub-complexes, or the entire complex. It could also be involved in the regulation of V-ATPase assembly/disassembly. Various dedicated V-ATPase chaperones and assembly/disassembly factors exist, and their knockdown or knockout results in incorrect folding and/or assembly of V-ATPase followed by its subsequent degradation and decreased abundance (14). For example, it has been shown recently that a kidney-specific inducible knockout of an essential chaperone for V-ATPase assembly, Atp6ap2, resulted in downregulation of V-ATPase levels and, therefore, function in kidney (43). To summarize we propose that Ncoa7 may also function as a V-ATPase chaperone in the kidney, and that its deletion results in V-ATPase destabilization and/or enhanced degradation of V-ATPase subunits leading to the overall downregulation of V-ATPase levels, and also to downregulation of other proteins involved in acid-base regulation, such as Car2 and AE1. Together, these effects result in the incomplete dRTA phenotype we describe here in *Ncoa7* KO mice.

Acknowledgements

We thank members of Dr. Warren Zapol's laboratory (Massachusetts General Hospital, Boston, MA) for assistance with using the Radiometer ABL800 FLEX for blood gas analysis.

Grants

558 This work was supported by NIH grants DK042956 (D.B.), DK097124 and HD040793 (S.B.)
559 and by Massachusetts General Hospital (MGH) Institutional support grants (D.B. and T.G.P.).
560 The MGH Program in Membrane Biology Microscopy Core receives additional support from the
561 Boston Area Diabetes and Endocrinology Research Center (DK57521) and the MGH Center for
562 the Study of Inflammatory Bowel Disease (DK43351). S.B. is a recipient of the Charles and Ann
563 Sanders Research Scholar Award at MGH. P.L.O is supported by a European Research Council
564 grant (PAROSIN, 311394). The Zeiss LSM800 microscope was acquired using an NIH Shared
565 Instrumentation Grant S10 OD021577-01.

566

567 **Disclosures**

568 None.

References

1. **Alper SL.** Familial renal tubular acidosis. *Journal of nephrology* 23 Suppl 16: S57-76, 2010.
2. **Alper SL, Natale J, Gluck S, Lodish HF, and Brown D.** Subtypes of intercalated cells in rat kidney collecting duct defined by antibodies against erythroid band 3 and renal vacuolar H⁺-ATPase. *Proceedings of the National Academy of Sciences of the United States of America* 86: 5429-5433, 1989.
3. **Bagnis C, Marshansky V, Breton S, and Brown D.** Remodeling the cellular profile of collecting ducts by chronic carbonic anhydrase inhibition. *American journal of physiology Renal physiology* 280: F437-448, 2001.
4. **Bastani B, Purcell H, Hemken P, Trigg D, and Gluck S.** Expression and distribution of renal vacuolar proton-translocating adenosine triphosphatase in response to chronic acid and alkali loads in the rat. *The Journal of clinical investigation* 88: 126-136, 1991.
5. **Bradley A, Anastassiadis K, Ayadi A, Battey JF, Bell C, Birling MC, Bottomley J, Brown SD, Burger A, Bult CJ, Bushell W, Collins FS, Desaintes C, Doe B, Economides A, Eppig JT, Finnell RH, Fletcher C, Fray M, Friendewey D, Friedel RH, Grosveld FG, Hansen J, Herault Y, Hicks G, Horlein A, Houghton R, Hrabe de Angelis M, Huylebroeck D, Iyer V, de Jong PJ, Kadin JA, Kaloff C, Kennedy K, Koutsourakis M, Lloyd KC, Marschall S, Mason J, McKerlie C, McLeod MP, von Melchner H, Moore M, Mujica AO, Nagy A, Nefedov M, Nutter LM, Pavlovic G, Peterson JL, Pollock J, Ramirez-Solis R, Rancourt DE, Raspa M, Remacle JE, Ringwald M, Rosen B, Rosenthal N, Rossant J, Ruiz Noppinger P, Ryder E, Schick JZ, Schnutgen F, Schofield P, Seisenberger C, Selloum M, Simpson EM, Skarnes WC, Smedley D, Stanford WL, Stewart AF, Stone K, Swan K, Tadepally H, Teboul L, Tocchini-Valentini GP, Valenzuela D, West AP, Yamamura K, Yoshinaga Y, and Wurst W.** The mammalian gene function resource: the International Knockout Mouse Consortium. *Mammalian genome : official journal of the International Mammalian Genome Society* 23: 580-586, 2012.
6. **Breton S, and Brown D.** Regulation of luminal acidification by the V-ATPase. *Physiology* 28: 318-329, 2013.
7. **Buckalew VM, Jr., McCurdy DK, Ludwig GD, Chaykin LB, and Elkinton JR.** Incomplete renal tubular acidosis. Physiologic studies in three patients with a defect in lowering urine pH. *The American journal of medicine* 45: 32-42, 1968.
8. **Dhayat NA, Schaller A, Albano G, Poindexter J, Griffith C, Pasch A, Gallati S, Vogt B, Moe OW, and Fuster DG.** The Vacuolar H⁺-ATPase B1 Subunit Polymorphism p.E161K Associates with Impaired Urinary Acidification in Recurrent Stone Formers. *Journal of the American Society of Nephrology : JASN* 27: 1544-1554, 2016.
9. **Dou H, Finberg K, Cardell EL, Lifton R, and Choo D.** Mice lacking the B1 subunit of H⁺ -ATPase have normal hearing. *Hearing research* 180: 76-84, 2003.
10. **Enerback S, Nilsson D, Edwards N, Heglind M, Alkanderi S, Ashton E, Deeb A, Kokash FEB, Bakhsh ARA, Van't Hoff W, Walsh SB, D'Arco F, Daryadel A, Bourgeois S, Wagner CA, Kleta R, Bockenhauer D, and Sayer JA.** Acidosis and Deafness in Patients with Recessive Mutations in FOXI1. *Journal of the American Society of Nephrology : JASN* 2017.

11. **Feldman M, Prikis M, Athanasiou Y, Elia A, Pierides A, and Deltas CC.** Molecular investigation and long-term clinical progress in Greek Cypriot families with recessive distal renal tubular acidosis and sensorineural deafness due to mutations in the ATP6V1B1 gene. *Clinical genetics* 69: 135-144, 2006.
12. **Finberg KE, Wagner CA, Bailey MA, Paunescu TG, Breton S, Brown D, Giebisch G, Geibel JP, and Lifton RP.** The B1-subunit of the H(+) ATPase is required for maximal urinary acidification. *Proceedings of the National Academy of Sciences of the United States of America* 102: 13616-13621, 2005.
13. **Finelli MJ, Sanchez-Pulido L, Liu KX, Davies KE, and Oliver PL.** The Evolutionarily Conserved Tre2/Bub2/Cdc16 (TBC), Lysin Motif (LysM), Domain Catalytic (TLDC) Domain Is Neuroprotective against Oxidative Stress. *The Journal of biological chemistry* 291: 2751-2763, 2016.
14. **Forgac M.** Vacuolar ATPases: rotary proton pumps in physiology and pathophysiology. *Nature reviews Molecular cell biology* 8: 917-929, 2007.
15. **Gomez J, Gil-Pena H, Santos F, Coto E, Arango A, Hernandez O, Rodriguez J, Nadal I, Cantos V, Chocron S, Vergara I, Madrid A, Vazquez C, Gonzalez LE, and Blanco F.** Primary distal renal tubular acidosis: novel findings in patients studied by next-generation sequencing. *Pediatric research* 79: 496-501, 2016.
16. **Halachmi S, Marden E, Martin G, MacKay H, Abbondanza C, and Brown M.** Estrogen receptor-associated proteins: possible mediators of hormone-induced transcription. *Science* 264: 1455-1458, 1994.
17. **Hennings JC, Picard N, Huebner AK, Stauber T, Maier H, Brown D, Jentsch TJ, Vargas-Poussou R, Eladari D, and Hubner CA.** A mouse model for distal renal tubular acidosis reveals a previously unrecognized role of the V-ATPase a4 subunit in the proximal tubule. *EMBO molecular medicine* 4: 1057-1071, 2012.
18. **Hurtado-Lorenzo A, Skinner M, El Annan J, Futai M, Sun-Wada GH, Bourgoin S, Casanova J, Wildeman A, Bechoua S, Ausiello DA, Brown D, and Marshansky V.** V-ATPase interacts with ARNO and Arf6 in early endosomes and regulates the protein degradative pathway. *Nature cell biology* 8: 124-136, 2006.
19. **Imai E, Kaneko S, Mori T, Okado T, Uchida S, and Tsukamoto Y.** A novel heterozygous mutation in the ATP6V0A4 gene encoding the V-ATPase a4 subunit in an adult patient with incomplete distal renal tubular acidosis. *Clinical kidney journal* 9: 424-428, 2016.
20. **Karet FE, Finberg KE, Nelson RD, Nayir A, Mocan H, Sanjad SA, Rodriguez-Soriano J, Santos F, Cremers CW, Di Pietro A, Hoffbrand BI, Winiarski J, Bakkaloglu A, Ozen S, Dusunsal R, Goodyer P, Hulton SA, Wu DK, Skvorak AB, Morton CC, Cunningham MJ, Jha V, and Lifton RP.** Mutations in the gene encoding B1 subunit of H+-ATPase cause renal tubular acidosis with sensorineural deafness. *Nature genetics* 21: 84-90, 1999.
21. **Lloyd KC.** A knockout mouse resource for the biomedical research community. *Annals of the New York Academy of Sciences* 1245: 24-26, 2011.
22. **Madsen KM, Verlander JW, Kim J, and Tisher CC.** Morphological adaptation of the collecting duct to acid-base disturbances. *Kidney international Supplement* 33: S57-63, 1991.
23. **Madsen KM, Verlander JW, and Tisher CC.** Relationship between structure and function in distal tubule and collecting duct. *Journal of electron microscopy technique* 9: 187-208, 1988.

24. **Merkulova M, Paunescu TG, Azroyan A, Marshansky V, Breton S, and Brown D.** Mapping the H(+) (V)-ATPase interactome: identification of proteins involved in trafficking, folding, assembly and phosphorylation. *Scientific reports* 5: 14827, 2015.
25. **Norgett EE, Golder ZJ, Lorente-Canovas B, Ingham N, Steel KP, and Karet Frankl FE.** Atp6v0a4 knockout mouse is a model of distal renal tubular acidosis with hearing loss, with additional extrarenal phenotype. *Proceedings of the National Academy of Sciences of the United States of America* 109: 13775-13780, 2012.
26. **Oliver PL, Finelli MJ, Edwards B, Bitoun E, Butts DL, Becker EB, Cheeseman MT, Davies B, and Davies KE.** Oxr1 is essential for protection against oxidative stress-induced neurodegeneration. *PLoS genetics* 7: e1002338, 2011.
27. **Palazzo V, Provenzano A, Becherucci F, Sansavini G, Mazzinghi B, Orlandini V, Giunti L, Roperto RM, Pantaleo M, Artuso R, Andreucci E, Bargiacchi S, Traficante G, Stagi S, Murer L, Benetti E, Emma F, Giordano M, Rivieri F, Colussi G, Penco S, Manfredini E, Caruso MR, Garavelli L, Andrulli S, Vergine G, Miglietti N, Mancini E, Malaventura C, Percesepe A, Grosso E, Materassi M, Romagnani P, and Giglio S.** The genetic and clinical spectrum of a large cohort of patients with distal renal tubular acidosis. *Kidney international* 2017.
28. **Paunescu TG, Da Silva N, Marshansky V, McKee M, Breton S, and Brown D.** Expression of the 56-kDa B2 subunit isoform of the vacuolar H(+)-ATPase in proton-secreting cells of the kidney and epididymis. *American journal of physiology Cell physiology* 287: C149-162, 2004.
29. **Paunescu TG, Da Silva N, Russo LM, McKee M, Lu HA, Breton S, and Brown D.** Association of soluble adenylyl cyclase with the V-ATPase in renal epithelial cells. *American journal of physiology Renal physiology* 294: F130-138, 2008.
30. **Paunescu TG, Jones AC, Tyszkowski R, and Brown D.** V-ATPase expression in the mouse olfactory epithelium. *American journal of physiology Cell physiology* 295: C923-930, 2008.
31. **Paunescu TG, Ljubojevic M, Russo LM, Winter C, McLaughlin MM, Wagner CA, Breton S, and Brown D.** cAMP stimulates apical V-ATPase accumulation, microvillar elongation, and proton extrusion in kidney collecting duct A-intercalated cells. *American journal of physiology Renal physiology* 298: F643-654, 2010.
32. **Paunescu TG, Rodriguez S, Benz E, McKee M, Tyszkowski R, Albers MW, and Brown D.** Loss of the V-ATPase B1 subunit isoform expressed in non-neuronal cells of the mouse olfactory epithelium impairs olfactory function. *PloS one* 7: e45395, 2012.
33. **Paunescu TG, Russo LM, Da Silva N, Kovacikova J, Mohebbi N, Van Hoek AN, McKee M, Wagner CA, Breton S, and Brown D.** Compensatory membrane expression of the V-ATPase B2 subunit isoform in renal medullary intercalated cells of B1-deficient mice. *American journal of physiology Renal physiology* 293: F1915-1926, 2007.
34. **Paunescu TG, Shum WW, Huynh C, Lechner L, Goetze B, Brown D, and Breton S.** High-resolution helium ion microscopy of epididymal epithelial cells and their interaction with spermatozoa. *Molecular human reproduction* 20: 929-937, 2014.
35. **Petryszak R, Keays M, Tang YA, Fonseca NA, Barrera E, Burdett T, Fullgrabe A, Fuentes AM, Jupp S, Koskinen S, Mannion O, Huerta L, Megy K, Snow C, Williams E, Barzine M, Hastings E, Weisser H, Wright J, Jaiswal P, Huber W, Choudhary J, Parkinson HE, and Brazma A.** Expression Atlas update--an integrated database of gene and protein expression in humans, animals and plants. *Nucleic acids research* 44: D746-752, 2016.

36. **Rodriguez Soriano J.** Renal tubular acidosis: the clinical entity. *Journal of the American Society of Nephrology : JASN* 13: 2160-2170, 2002.
37. **Roy JW, Hill E, Ruan YC, Vedovelli L, Paunescu TG, Brown D, and Breton S.** Circulating aldosterone induces the apical accumulation of the proton pumping V-ATPase and increases proton secretion in clear cells in the caput epididymis. *American journal of physiology Cell physiology* 305: C436-446, 2013.
38. **Schneider CA, Rasband WS, and Eliceiri KW.** NIH Image to ImageJ: 25 years of image analysis. *Nature methods* 9: 671-675, 2012.
39. **Shao W, Halachmi S, and Brown M.** ERAP140, a conserved tissue-specific nuclear receptor coactivator. *Molecular and cellular biology* 22: 3358-3372, 2002.
40. **Smith AN, Borthwick KJ, and Karet FE.** Molecular cloning and characterization of novel tissue-specific isoforms of the human vacuolar H(+)-ATPase C, G and d subunits, and their evaluation in autosomal recessive distal renal tubular acidosis. *Gene* 297: 169-177, 2002.
41. **Smith AN, Skaug J, Choate KA, Nayir A, Bakkaloglu A, Ozen S, Hulton SA, Sanjad SA, Al-Sabban EA, Lifton RP, Scherer SW, and Karet FE.** Mutations in ATP6N1B, encoding a new kidney vacuolar proton pump 116-kD subunit, cause recessive distal renal tubular acidosis with preserved hearing. *Nature genetics* 26: 71-75, 2000.
42. **Stover EH, Borthwick KJ, Bavalia C, Eady N, Fritz DM, Rungroj N, Giersch AB, Morton CC, Axon PR, Akil I, Al-Sabban EA, Baguley DM, Bianca S, Bakkaloglu A, Bircan Z, Chauveau D, Clermont MJ, Guala A, Hulton SA, Kroes H, Li Volti G, Mir S, Mocan H, Nayir A, Ozen S, Rodriguez Soriano J, Sanjad SA, Tasic V, Taylor CM, Topaloglu R, Smith AN, and Karet FE.** Novel ATP6V1B1 and ATP6V0A4 mutations in autosomal recessive distal renal tubular acidosis with new evidence for hearing loss. *Journal of medical genetics* 39: 796-803, 2002.
43. **Trepiccione F, Gerber SD, Grahammer F, Lopez-Cayuqueo KI, Baudrie V, Paunescu TG, Capen DE, Picard N, Alexander RT, Huber TB, Chambrey R, Brown D, Houillier P, Eladari D, and Simons M.** Renal Atp6ap2/(Pro)renin Receptor Is Required for Normal Vacuolar H+-ATPase Function but Not for the Renin-Angiotensin System. *Journal of the American Society of Nephrology : JASN* 27: 3320-3330, 2016.
44. **Vedovelli L, Rothermel JT, Finberg KE, Wagner CA, Azroyan A, Hill E, Breton S, Brown D, and Paunescu TG.** Altered V-ATPase expression in renal intercalated cells isolated from B1 subunit-deficient mice by fluorescence-activated cell sorting. *American journal of physiology Renal physiology* 304: F522-532, 2013.
45. **Wrong O, and Davies HE.** The excretion of acid in renal disease. *The Quarterly journal of medicine* 28: 259-313, 1959.
46. **Zhang J, Fuster DG, Cameron MA, Quinones H, Griffith C, Xie XS, and Moe OW.** Incomplete distal renal tubular acidosis from a heterozygous mutation of the V-ATPase B1 subunit. *American journal of physiology Renal physiology* 307: F1063-1071, 2014.

Figure Captions.

Figure 1. Confirmation of the deletion of critical regions of *Ncoa7* gene in *Ncoa7* knockout mice.

(A) Schematic representation of the gene targeting strategy used to generate *Ncoa7* KO mice as part of the Knockout Mouse Project KOMP2-DTCC (<https://www.komp.org/>). From top to bottom: *Ncoa7* wild-type allele, targeting vector and targeted alleles tm1 and tm1.1. Exon-intron boundaries of *Ncoa7* wild-type allele are shown based on its 5105 bp transcript *Ncoa7*-201 (Ensembl, ENSMUST00000068567). This transcript maps to a region located at mouse chromosome 10: 30,645,584-30,803,107 reverse strand (Genome Build GRCm38:CM001003.2) which contains 16 exons; the first exon is non-coding, the remaining 15 exons (2 through 16) are coding. The *Ncoa7* targeting vector contains a ZEN-Ub1 cassette bearing a *lacZ* reporter and a neomycin (neo) selectable marker flanked by loxP sites. The 5' arm of the *Ncoa7* targeting vector is homologous to a 15001 bp intronic sequence between *Ncoa7* exons 1 and 2 and its 3' arm is homologous to a 15001 bp intronic sequence between *Ncoa7* exons 3 and 4. Targeted allele tm1 was created by homologous recombination which resulted in the insertion of the ZEN-Ub1 cassette and a 49126 bp deletion in the *Ncoa7* wild-type gene, spanning coding exons 2 and 3 and the intronic sequence between them. Targeted allele tm1.1 was created by Cre-mediated removal of the neo resistance marker from the parental tm1 allele. For further details see Materials and Methods. Positions of forward and reverse primer pairs used for mouse genotyping (F1/R1 and F2/R2) and end-point RT-PCR (F3/R3) are indicated. ZEN-Ub1 cassette and all primers are not drawn to scale.

(B) Representative PCR analysis of genomic DNA extracted from tails of wild-type (+/+), heterozygous (+/-) and homozygous (-/-) *Ncoa7* KO mice (genotyping). For each sample, two

766 separate PCR reactions using either F1/R1 or F2/R2 primer pairs were run. Primer pair F1/R1 is
767 specific for the wild-type allele and amplifies a 173 bp DNA fragment located in the intronic
768 sequence between *Ncoa7* exons 2 and 3. Primer pair F2/R2 is specific for targeted alleles and in
769 the tm1.1 allele amplifies a 580 bp fragment spanning part of the *lacZ* sequence, the loxP site
770 and part of the intronic sequence between *Ncoa7* exons 3 and 4. The inferred genotypes are
771 shown above. M - marker, 100 bp DNA ladder.

772 (C) Absence of *Ncoa7* full-length transcripts in *Ncoa7* KO mice was confirmed by end-point RT-
773 PCR using an F3/R3 primer pair, which is specific for *Ncoa7* exon 3 and amplifies an 82 bp
774 fragment within this exon. Total RNA was isolated from four WT (+/+, 1-4) and four
775 homozygous (-/-, 5-8) mouse kidneys and reverse transcribed. RT products were used as
776 templates for PCR with primer pairs specific for either *Ncoa7* (F3/R3) or *Rpl19* (ribosomal
777 protein L19) sequence, used as a loading control. NC - negative (no template) control. M -
778 marker, 100 bp DNA ladder.

779 (D) Absence of *Ncoa7* protein in *Ncoa7* KO mice was confirmed by Western blotting. Total
780 protein lysates were prepared from four WT and four *Ncoa7* KO mouse kidneys. Arrow points to
781 the full-length *Ncoa7* protein of ~140 kDa molecular weight (MW). The lower molecular weight
782 (LMW) proteins, in particular ~76 kDa and 100 kDa, detected in both WT and *Ncoa7* KO mice
783 are apparently non-specific, while other LMW proteins, present only in WT mice could be
784 *Ncoa7* degradation products.

785 (E) The full-length 140 kDa *Ncoa7* protein, but not the LMW proteins, interacts with B1 subunit
786 of V-ATPase in kidney. Proteins were co-immunoprecipitated by anti-B1 antibodies from whole
787 kidney lysates and then detected by antibodies against *Ncoa7*. Note, that heavy chains of

antibodies (HC) and heavy plus light chains of antibodies (HC+LC) are also detected in both the antibodies (Abs) only control lane, as well as in the anti-B1 immunoprecipitation (IP) lane. (F,G) *Ncoa7* is absent from intercalated cells in *Ncoa7* KO mouse kidney. Overview immunofluorescence micrographs of inner stripe regions of WT (F) and *Ncoa7* KO (G) kidney sections, double-stained with antibodies against the A subunit of V-ATPase (green) and *Ncoa7* (red). ICs are present in collecting ducts. The other, unstained tubules are thick ascending limbs of Henle. Scale bar = 20 μ m.

Figure 2. *Ncoa7* KO mice demonstrate defective urinary acidification and develop hypobicarbonatemia without acidemia after acid loading with ammonium chloride. Conversely, *Ncoa7* KO mice did not develop significant hyperbicarbonatemia and alkalemia after alkali loading with sodium bicarbonate. (A) On a standard rodent diet blood pH is normal in *Ncoa7* KO mice and not significantly different from WT controls. Blood pH did not change significantly in either WT or *Ncoa7* KO mice after acid loading with 0.28 M NH_4Cl for 3 days. Blood pH increased significantly in WT but not in *Ncoa7* KO mice after alkali loading with 0.28 M NaHCO_3 for 3 days (B) Serum HCO_3^- levels were similar in WT and *Ncoa7* KO mice maintained on a standard diet. After acid loading, serum HCO_3^- levels were reduced in mice of both genotypes, but were significantly lower only in *Ncoa7* KO mice ($p = 0.001$ standard diet vs. acid load). After alkali loading, serum HCO_3^- levels were increased in mice of both genotypes, but were significantly higher only in WT mice ($p < 0.01$ standard diet vs. alkali load). (C) Urine pH was significantly higher in *Ncoa7* KO mice compared to WT controls on a standard diet ($p < 0.0001$ WT vs. *Ncoa7* KO) and after both acid ($p < 0.0001$) and alkali ($p < 0.05$) loading. Note, that while acid loading resulted in a more acidic urine pH in mice of both genotypes, pH remained significantly higher in *Ncoa7* KO than in WT mice. Alkali loading resulted in a

significantly higher alkaline urine pH in WT mice and an even greater alkaline urine pH in *Ncoa7* KO mice. All values are means \pm SEM. * is for p-value < 0.05, ** is for p-value < 0.01, *** is for p-value < 0.001, **** is for p-value < 0.0001; t-test. The actual p-values and other details can be found in Tables 1 and 2.

Figure 3. The abundance of B1, B2, A, and a4 subunits of V-ATPase (Atp6v1b1, Atp6v1b2, Atp6v1a and Atp6v0a4), carbonic anhydrase 2 (Ca2) and the anion exchanger 1 (Slc4a1) is decreased in the medulla of *Ncoa7* KO compared to WT mice. (A) Representative western blots showing abundance of the indicated subunits of V-ATPase, Ca2 and Slc4a1 in protein lysates of kidney medulla of WT and *Ncoa7* KO mice (n=4 per genotype). A representative image of Ponceau S-stained membrane demonstrates equal protein loading in all samples. (B) Quantification of western blotting results by band densitometry analysis. All values are means \pm SEM. The actual p-values are shown ; t-test.

Figure 4. By immunofluorescence, levels of A and B2 subunits of V-ATPase (Atp6v1a and Atp6v1b2) are downregulated in intercalated cells (ICs) in kidney collecting ducts from the inner stripe (IS) of the outer medulla in *Ncoa7* KO mice compared to WT controls. Overview confocal micrographs of IS regions of WT (A-C) and *Ncoa7* KO (D-F) kidney sections, double-stained with antibodies against the A subunit (red, A and D) and B2 subunit of V-ATPase (green, B and E). Merged images (C and F) show co-expression and partial co-localization of A (red) and B2 (green) subunits of V-ATPase in ICs of both WT (C) and *Ncoa7* KO (F) mice, as expected. The anti-A subunit antibody clearly distinguishes ICs in IS in both WT and *Ncoa7* KO mice. Staining with both anti-A (red) and anti-B2 (green) V-ATPase subunit antibodies is weaker in *Ncoa7* KOs

(D and E) than in WT mice (A and B); the B2 subunit is barely detectable in ICs of the *Ncoa7* KO mouse kidney (E, F). Note, that tubules with uniform punctate subapical staining for B2 subunit of V-ATPase in both WT (green, B and C) and *Ncoa7* KO (green, E and F) mice are thick ascending limbs. Scale bar = 20 μ m.

Figure 5. Increased size and appearance of some continuous rows of intercalated cells (ICs) in kidney collecting ducts from the inner stripe (IS) of the outer medulla in *Ncoa7* KO mice compared to WT controls. Overview micrographs of IS regions of WT (A and C) and *Ncoa7* KO (B and D) kidney sections, single-stained with an antibody against the A subunit of V-ATPase (green, A and B) or double-stained with antibodies against the B1 subunit of V-ATPase (green, C and D) and AE1 (red, C and D). Arrows in B indicate continuous rows of adjacent ICs in the IS of *Ncoa7* KO mice, that are not seen in WT mice. Arrowheads in C and D point to the collecting duct tubules magnified in the inset panels. Nuclei are counterstained with 4',6-diamidino-2-phenylindole, dihydrochloride (DAPI, blue). Note that this figure does not reflect the quantitative difference in V-ATPase levels in *Ncoa7* KO in comparison with WT mice, because images from different genotypes were not acquired under identical conditions in order to better show the rows of cells in the *Ncoa7* KO mouse. Scale bar = 20 μ m.

Figure 6. Number of intercalated cells in both the inner stripe (IS) of the outer medulla and the inner medulla (IM) does not change in *Ncoa7* KO mice in comparison with WT controls. Quantification was performed on digital epifluorescence images of the entire IS of the outer medullary region (A) and the proximal 2 mm² region of the IM (B). All values are means \pm SEM. NS – non-significant. The actual p-values can be found in the “Results” section.

857
858 **Figure 7.** Ultrastructural (EM) details of morphologic differences between intercalated cells
859 (ICs) from the inner stripe (IS) of outer medulla of WT and *Ncoa7* KO kidney collecting ducts.
860 Upper panels: overviews of representative collecting ducts from IS of WT (A) and *Ncoa7* KO
861 (B) mice. Panel B shows adjacent ICs, never seen in WT IS collecting ducts; arrows point to the
862 distorted principal cells squeezed by the oversized ICs. The black square boxes in panels A and
863 B indicate the area magnified in the panels C and D, respectively. Lower panels: High
864 magnification images showing morphologic appearance of IS ICs from WT (C) and *Ncoa7* KO
865 (D) mice. Arrowhead in panel D points to the tight junction between two adjacent ICs. Note, that
866 *Ncoa7* KO ICs have an enlarged apical membrane region, which protrudes into the lumen and
867 contains numerous well-developed microvilli, while WT IC cells are flatter and have very few
868 microvilli, but numerous sub-apical vesicles that characterize this cell type. Compared to WT
869 cells, the total apical surface is greatly increased in *Ncoa7* KO ICs, indicating that typical ICs in
870 the *Ncoa7* KO kidneys are more activated compared to typical WT ICs. Scale bar = 2 μ m.

871
872 **Figure 8.** V-ATPase localizes predominantly in the apical microvilli in *Ncoa7* KO intercalated
873 cells (ICs). (A) Low magnification overview image of a representative collecting duct from inner
874 stripe of *Ncoa7* KO mouse. Arrow indicates cell region magnified in panel B. (B) Higher
875 magnification image showing numerous immunogold particles labeling V-ATPase in the well
876 developed apical microvilli and to a lesser extent in the of sub-apical vesicles of this typical
877 *Ncoa7* KO IC. Scale bar = 2 μ m.

878

879 **Figure 9.** Size of intercalated cells (ICs) is significantly increased in *Ncoa7* KO mice in
880 comparison with WT controls. Quantification was performed on transmission electron
881 microscopy images. An average 40% increase in the area of ICs was measured in kidneys of
882 *Ncoa7* KO mice. All values are means \pm SEM.

Table 1. Summary of NH₄Cl –loading of mice. Venous blood gases and pH, serum electrolytes and urine pH and osmolality of wild-type and *Ncoa7* knockout mice on a standard rodent diet and after acid loading with 0.28 M NH₄Cl for 3 days.

	Standard diet			Acid load			<i>P</i> (+/+ standard vs. +/+ acidified)	<i>P</i> (-/- standard vs. -/- acidified)
	+/+	-/-	<i>P</i> (+/+ standard vs. -/- standard)	+/+	-/-	<i>P</i> (+/+ acidified vs. -/- acidified)		
Venous pH	7.26 ± 0.02 (11)	7.26 ± 0.02 (12)	0.9541	7.23 ± 0.03 (8)	7.22 ± 0.04 (8)	0.9014	0.3118	0.2816
pCO ₂ (mmHg)	46.24 ± 1.31 (11)	46.52 ± 0.60 (12)	0.8435	43.43 ± 2.14 (8)	36.46 ± 2.17 (8)	0.0384 (*)	0.2536	<0.0001 (****)
HCO ₃ ⁻ , mM	20.31 ± 0.84 (11)	20.43 ± 0.81 (12)	0.9161	17.58 ± 1.17 (8)	14.71 ± 1.31 (8)	0.1255	0.0678	0.001 (***)
Na ⁺ , mM	151.4 ± 0.92 (11)	152.3 ± 0.25 (8)	0.4333	157.5 ± 1.7 (8)	155.3 ± 1.0 (8)	0.2663	0.0031 (**)	0.0101 (*)
K ⁺ , mM	4.3 ± 0.27 (7)	4.2 ± 0.21 (6)	0.7834	4.06 ± 0.18 (8)	4.53 ± 0.29 (6)	0.1770	0.4733	0.3766
Cl ⁻ , mM	114.8 ± 1.08 (11)	117.1 ± 0.72 (8)	0.1202	123.9 ± 1.84 (8)	124.0 ± 1.49 (8)	0.9586	0.0003 (***)	0.001 (***)
Urine pH	6.15 ± 0.08 (22)	6.98 ± 0.13 (20)	<0.0001 (****)	5.57 ± 0.03 (17)	5.86 ± 0.04 (18)	<0.0001 (****)	<0.0001 (****)	<0.0001

Urine osmolality, mmol/kg	2267 ± 227 (11)	2584 ± 188 (11)	0.295	3398 ± 150 (4)	3323 ± 225 (3)	0.781	0.013 (*)	0.079
Water intake, ml/g BW	0.18 ± 0.03 (8)	0.15 ± 0.01 (6)	0.4044	0.17 ± 0.01 (4)	0.15 ± 0.01 (4)	0.4223	0.7558	0.9671
NH ₄ Cl load, mmoles/g BW	N/A	N/A	N/A	0.046 ± 0.003 (4)	0.042 ± 0.003 (4)	0.4223	N/A	N/A

All values are means ± SEM. Numbers of animals are in parentheses. * is for p-value < 0.05, **

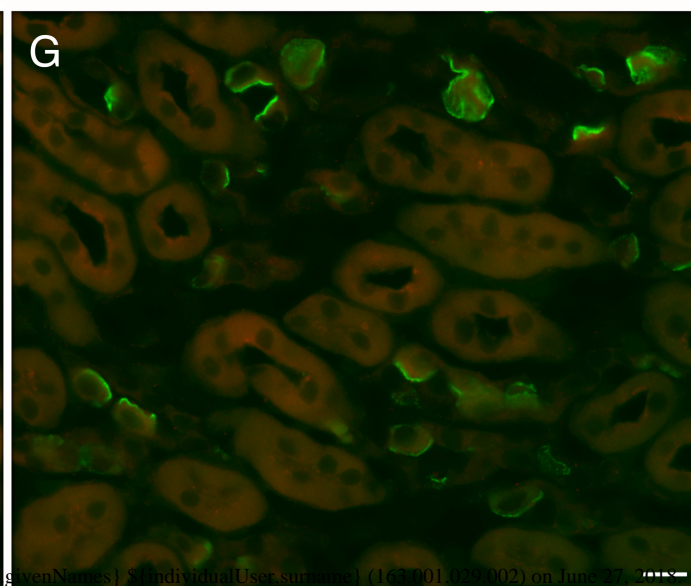
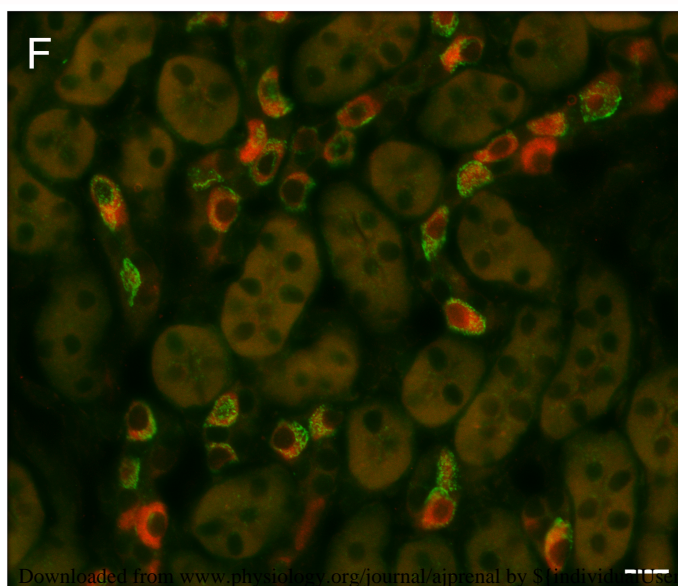
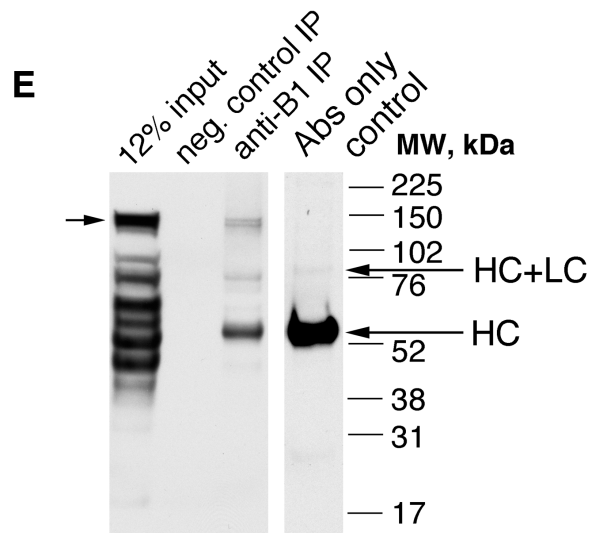
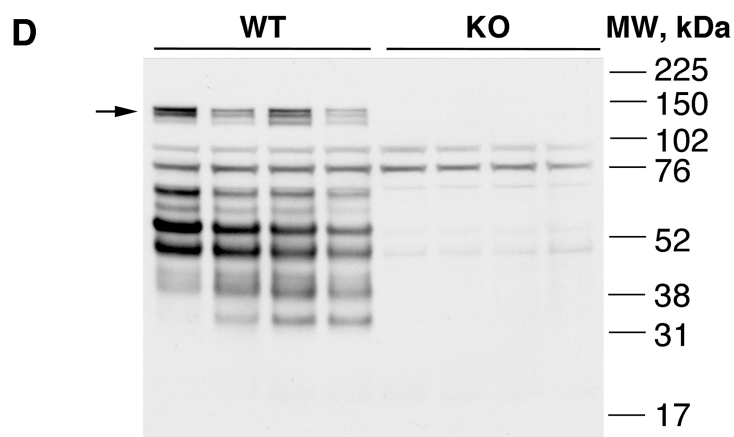
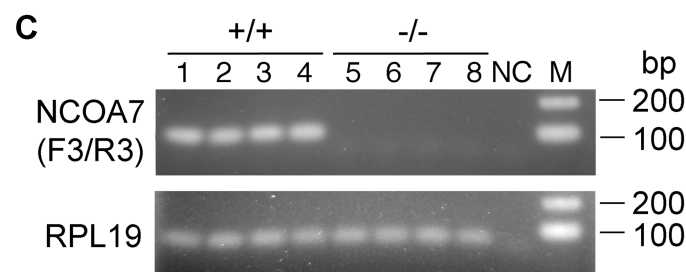
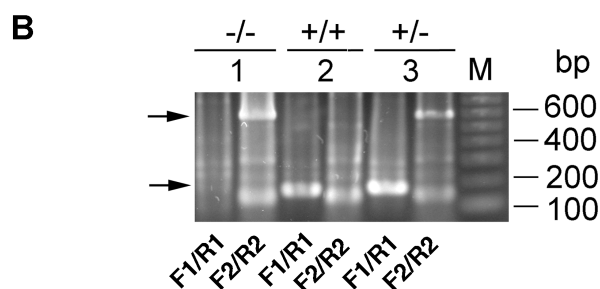
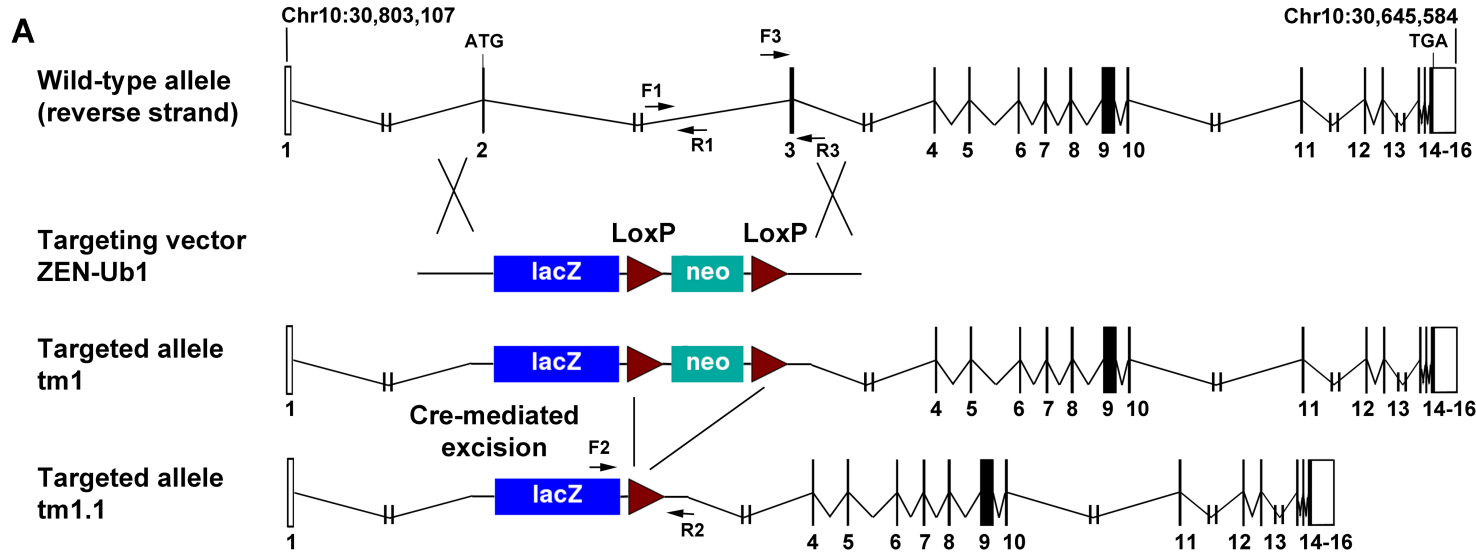
is for p-value < 0.01, *** is for p-value < 0.001, **** is for p-value < 0.0001; t-test. N/A = not applicable.

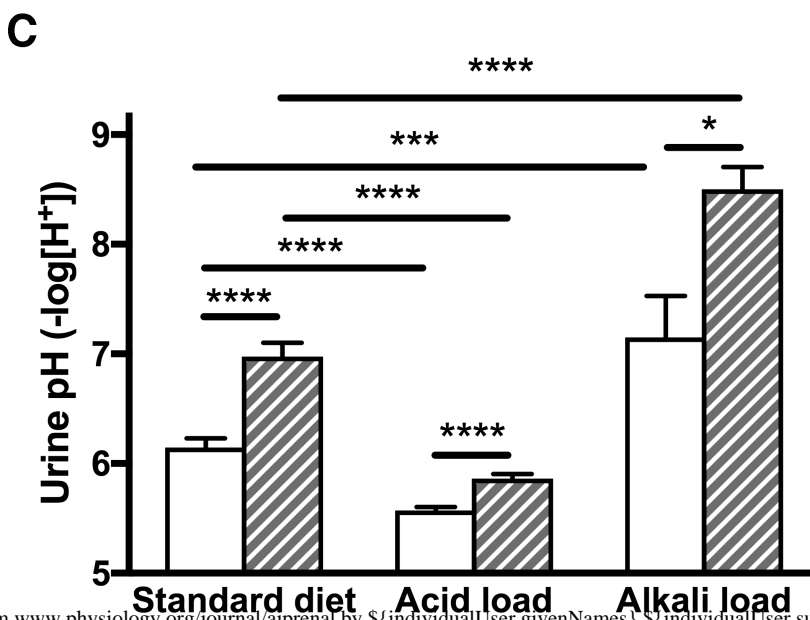
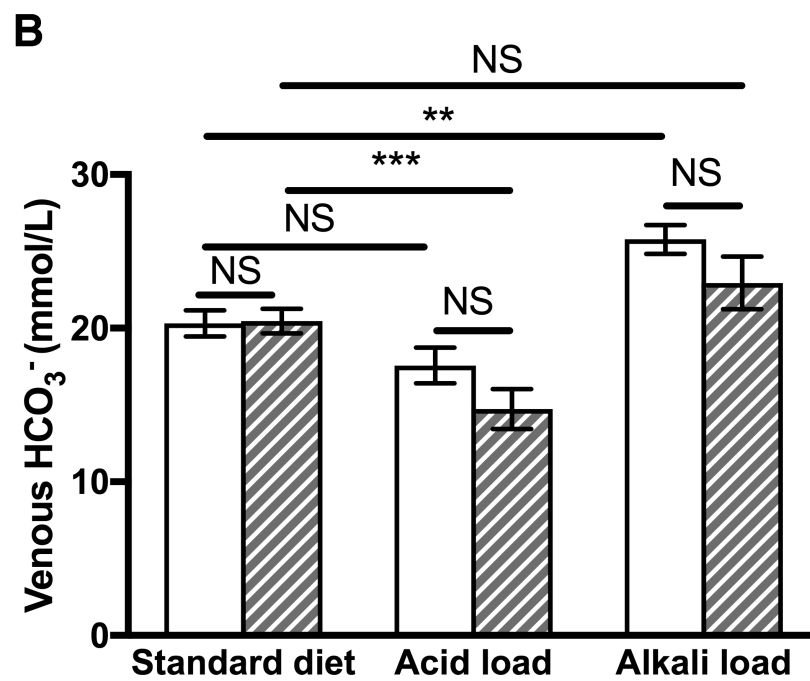
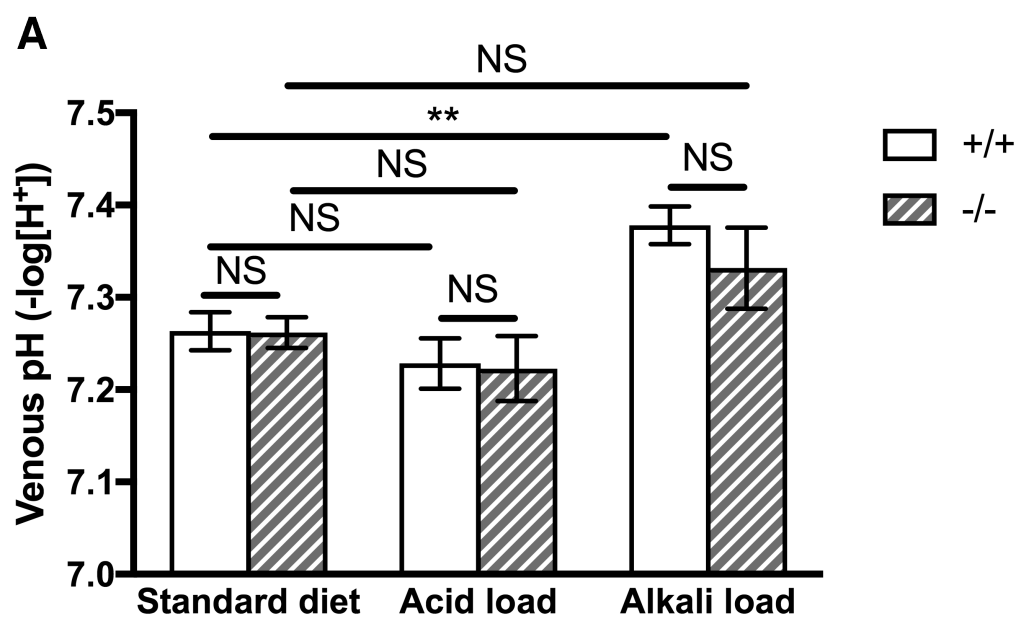
Table 2. Summary of NaHCO₃-loading of mice. Venous blood gases and pH, serum electrolytes and urine pH and osmolality of wild-type and *Ncoa7* knockout mice on a standard rodent diet and after alkali loading with 0.28 M NaHCO₃ for 3 days.

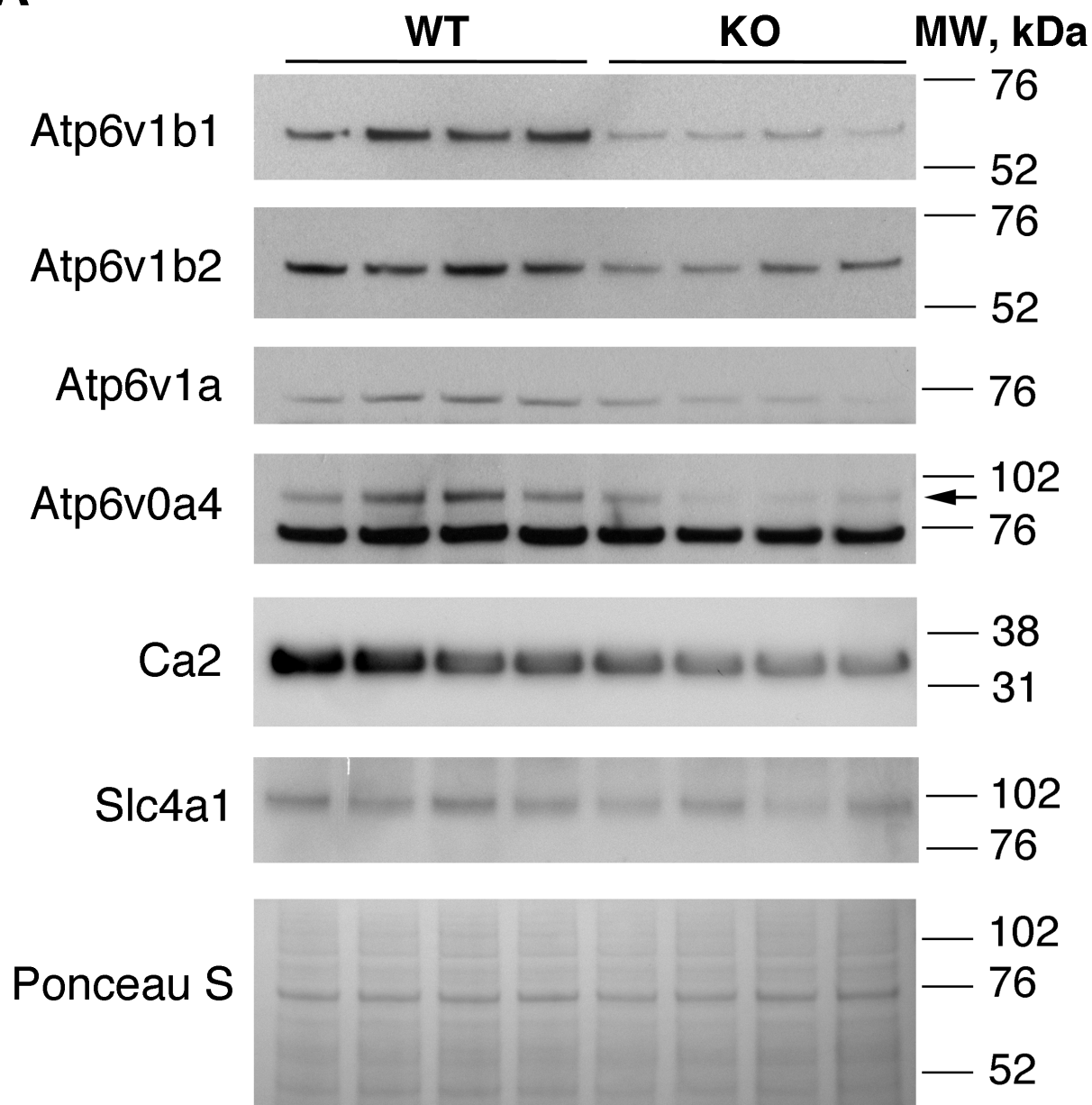
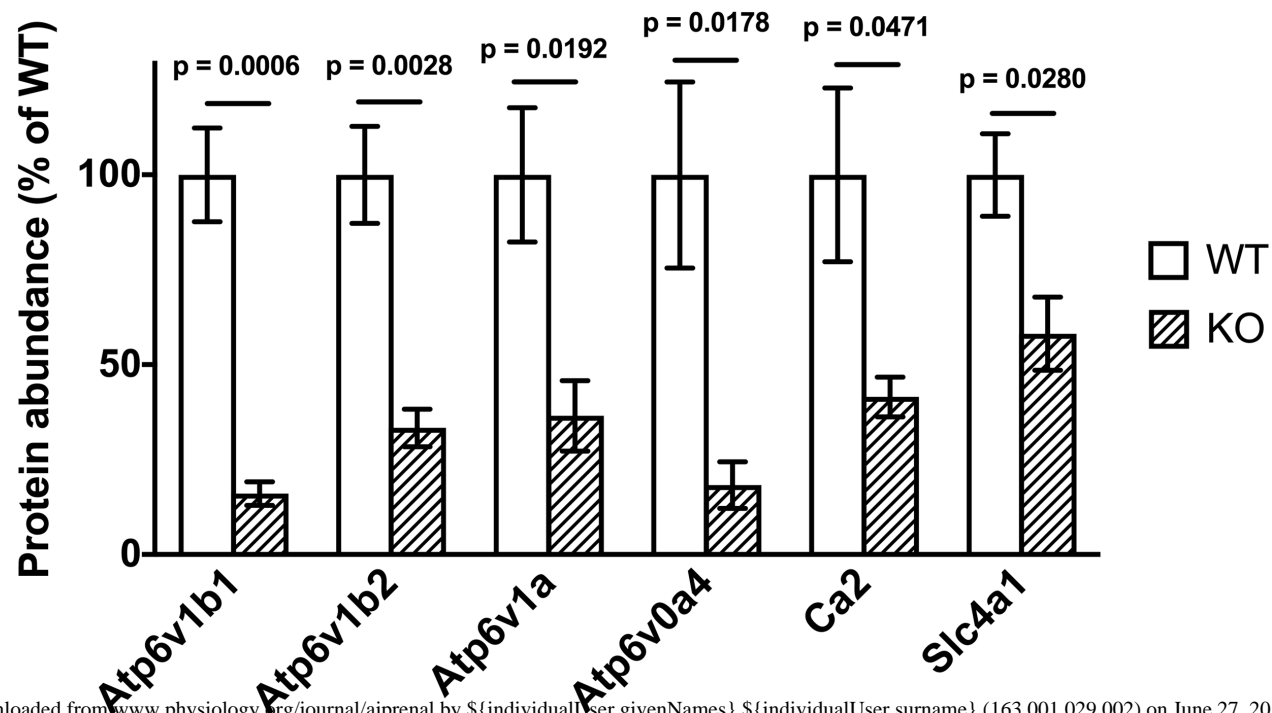
	Alkali load			<i>P</i> (+/+ standard (from Table 1) vs. +/+ alkalinized)	<i>P</i> (-/- standard (from Table 1) vs. -/- alkalinized)
	+/+	-/-	<i>P</i> (+/+ alkalinized vs. -/- alkalinized)		
Venous pH	7.38 ± 0.02 (4)	7.33 ± 0.04 (4)	0.3773	0.0084 (**)	0.0871
pCO ₂ (mmHg)	44.75 ± 0.64 (4)	44.2 ± 1.52 (4)	0.7495	0.5223	0.1043
HCO ₃ ⁻ , mM	25.78 ± 0.93 (4)	22.93 ± 1.71 (4)	0.1937	0.0033 (**)	0.1641
Na ⁺ , mM	151.50 ± 0.50 (4)	152.8 ± 0.48 (4)	0.2110	0.9327	0.3260
K ⁺ , mM	4.65 ± 0.17 (4)	4.00 ± 0.37 (4)	0.1633	0.3919	0.6277
Cl ⁻ , mM	113.0 ± 1.29 (4)	114.0 ± 1.96 (4)	0.6847	0.3723	0.0918
Urine pH	7.15 ± 0.04 (4)	8.5 ± 0.20 (4)	0.0199 (*)	0.0004 (***)	<0.0001 (****)

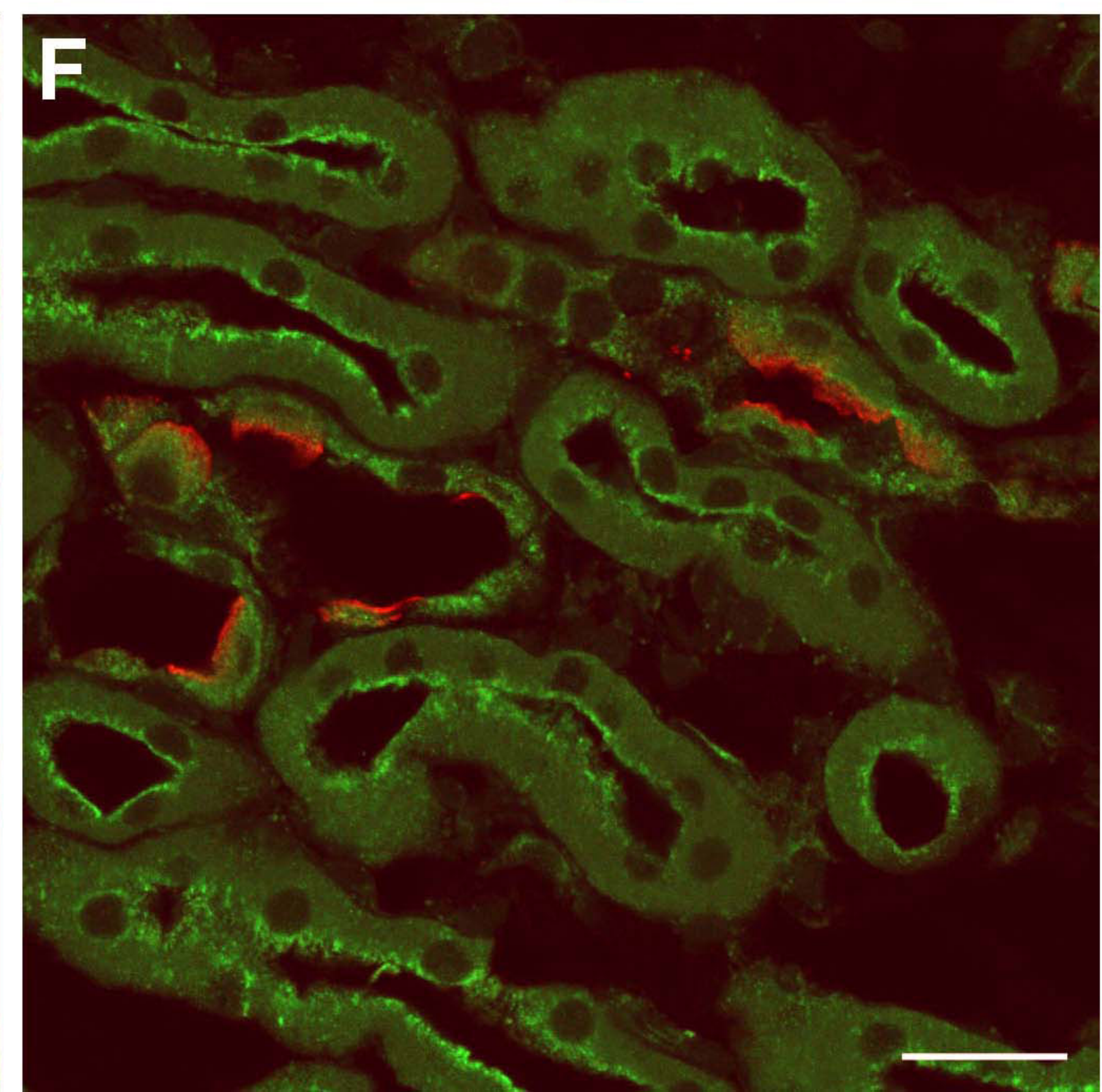
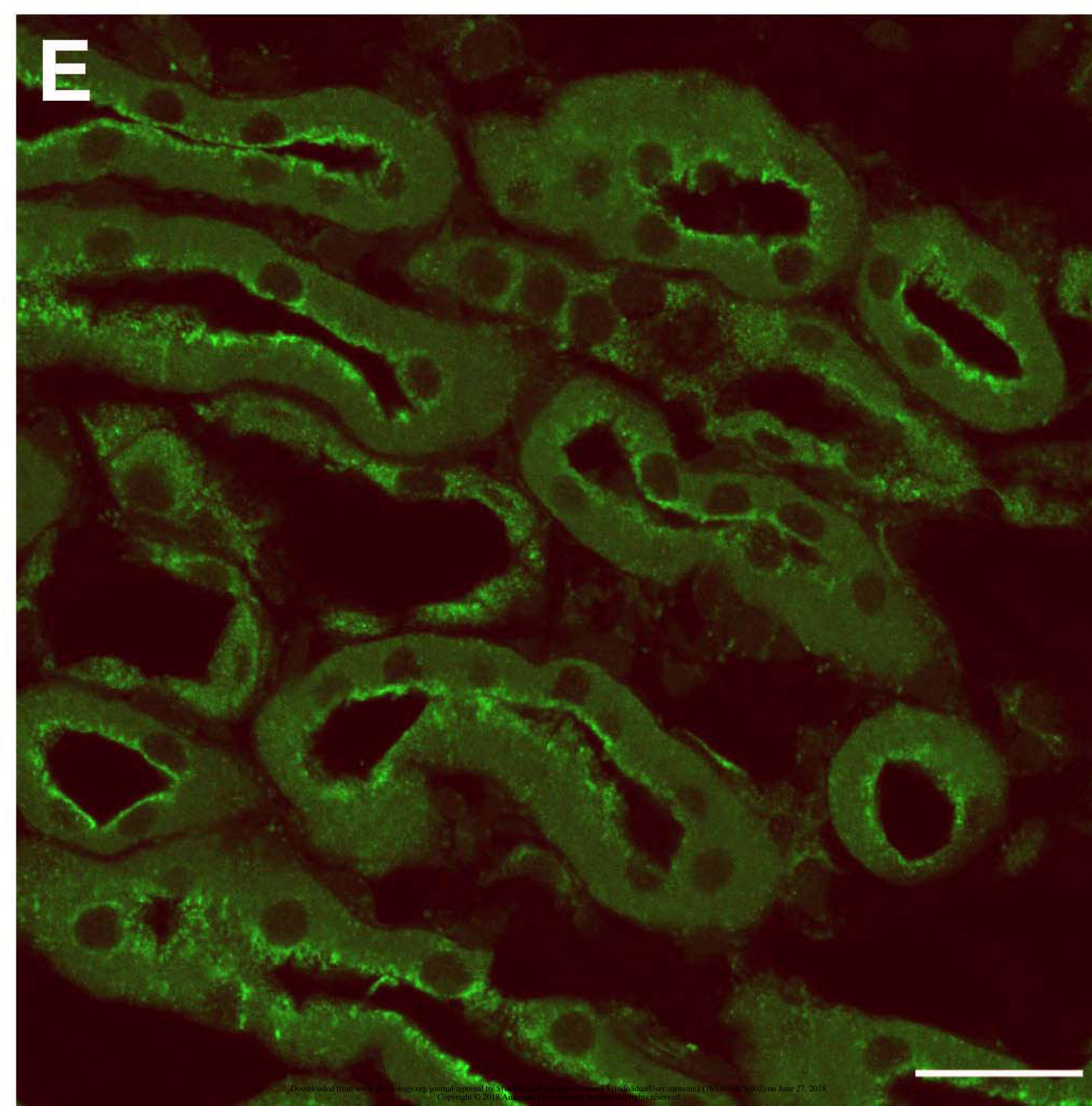
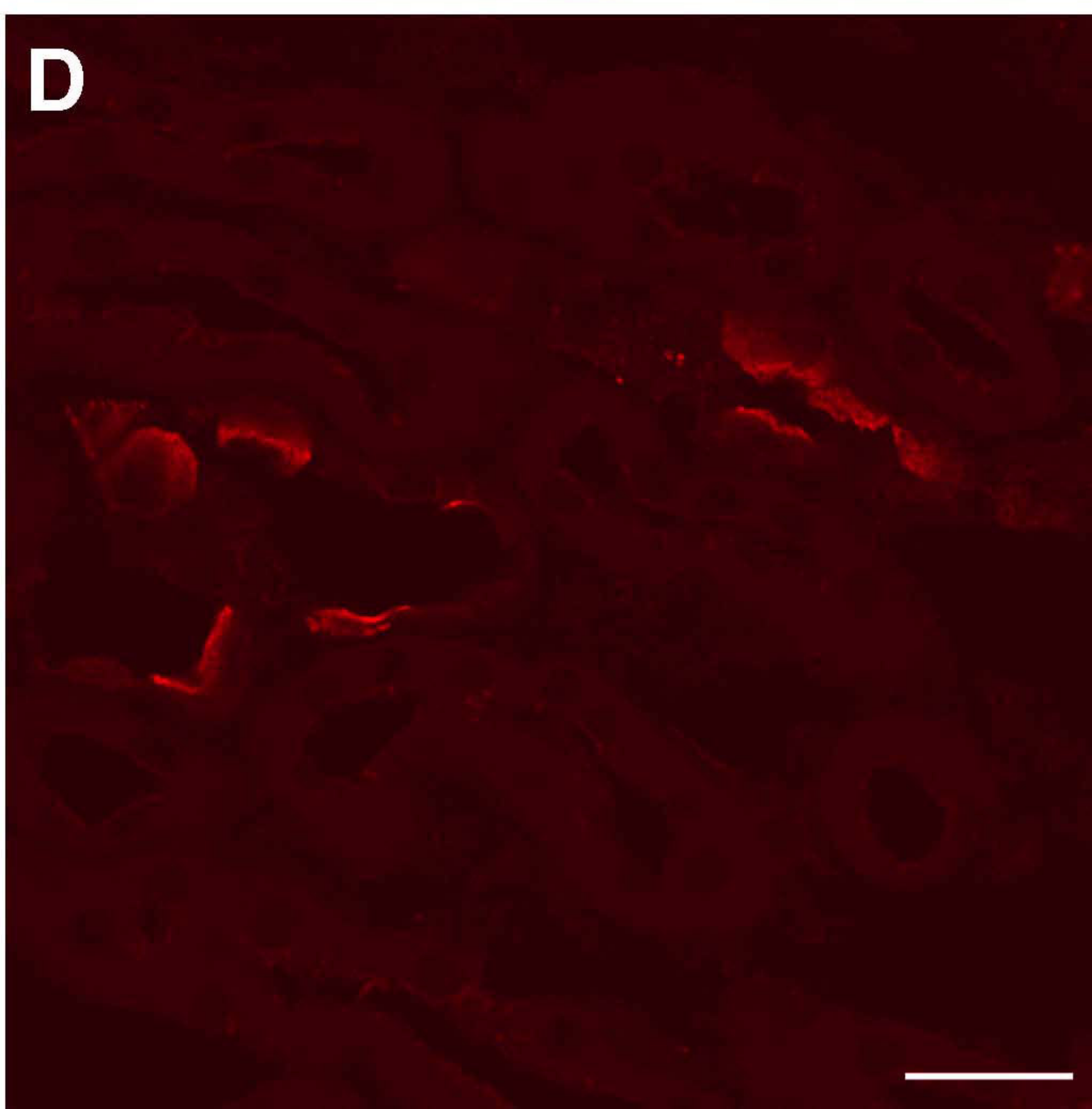
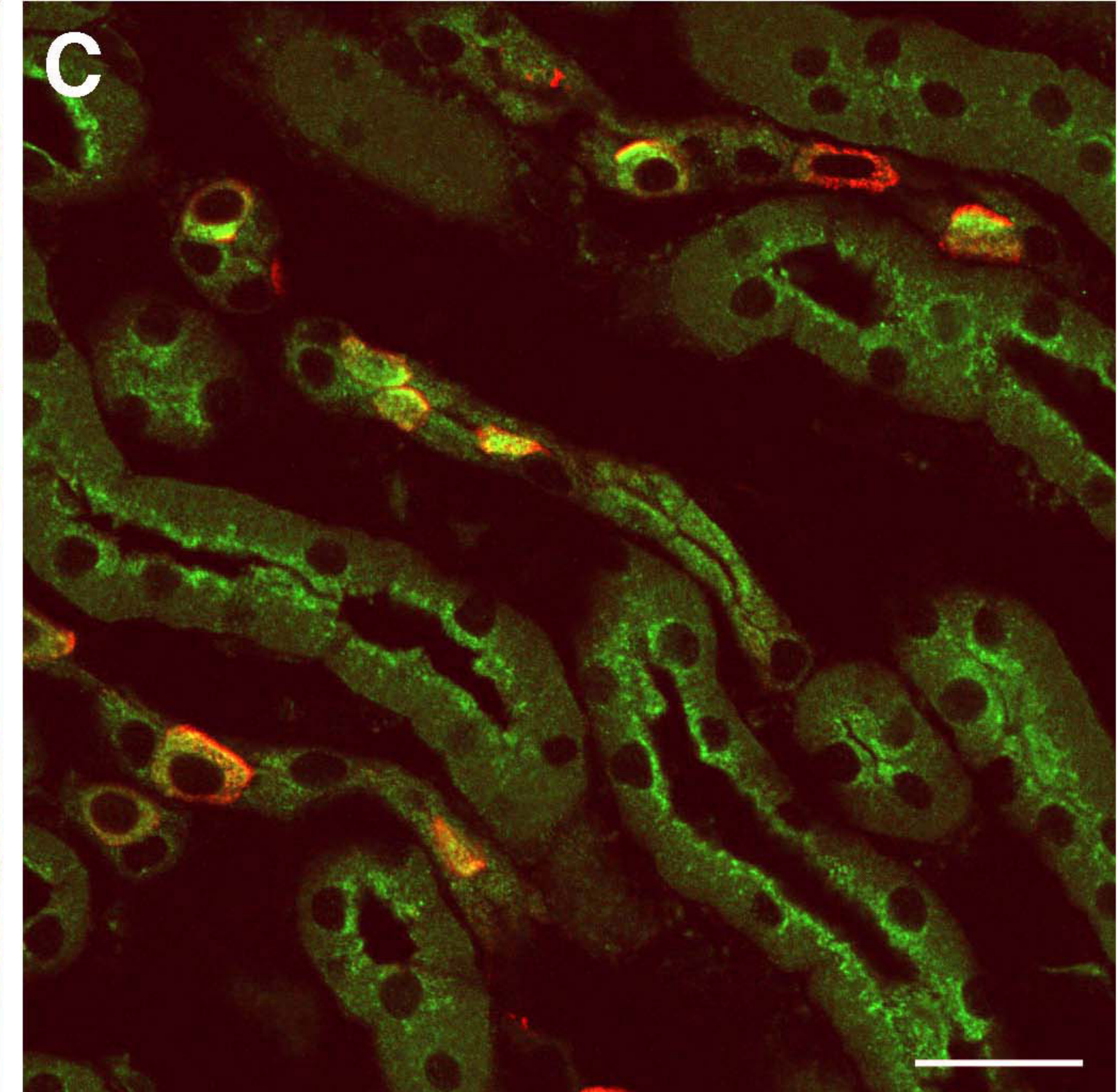
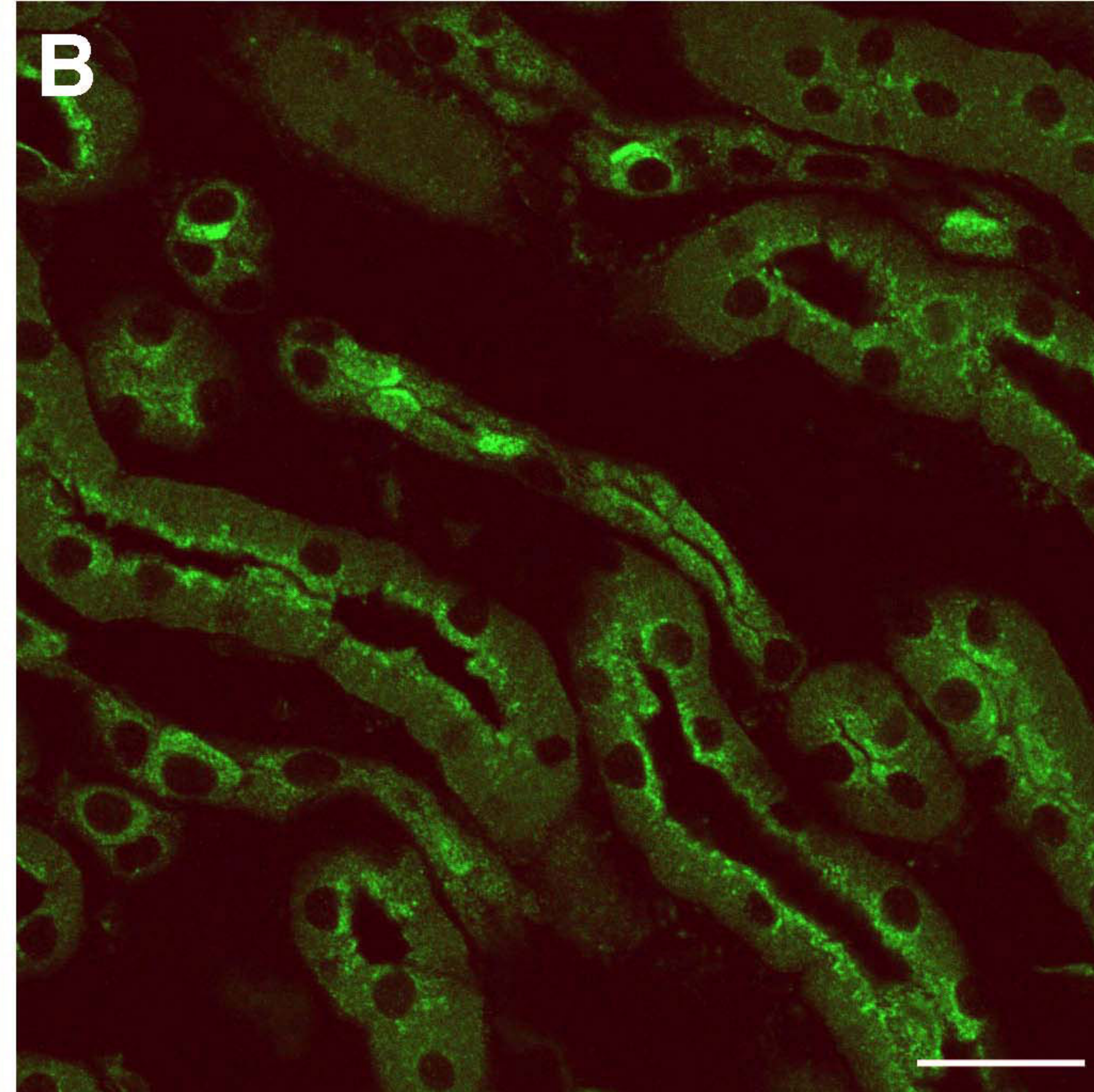
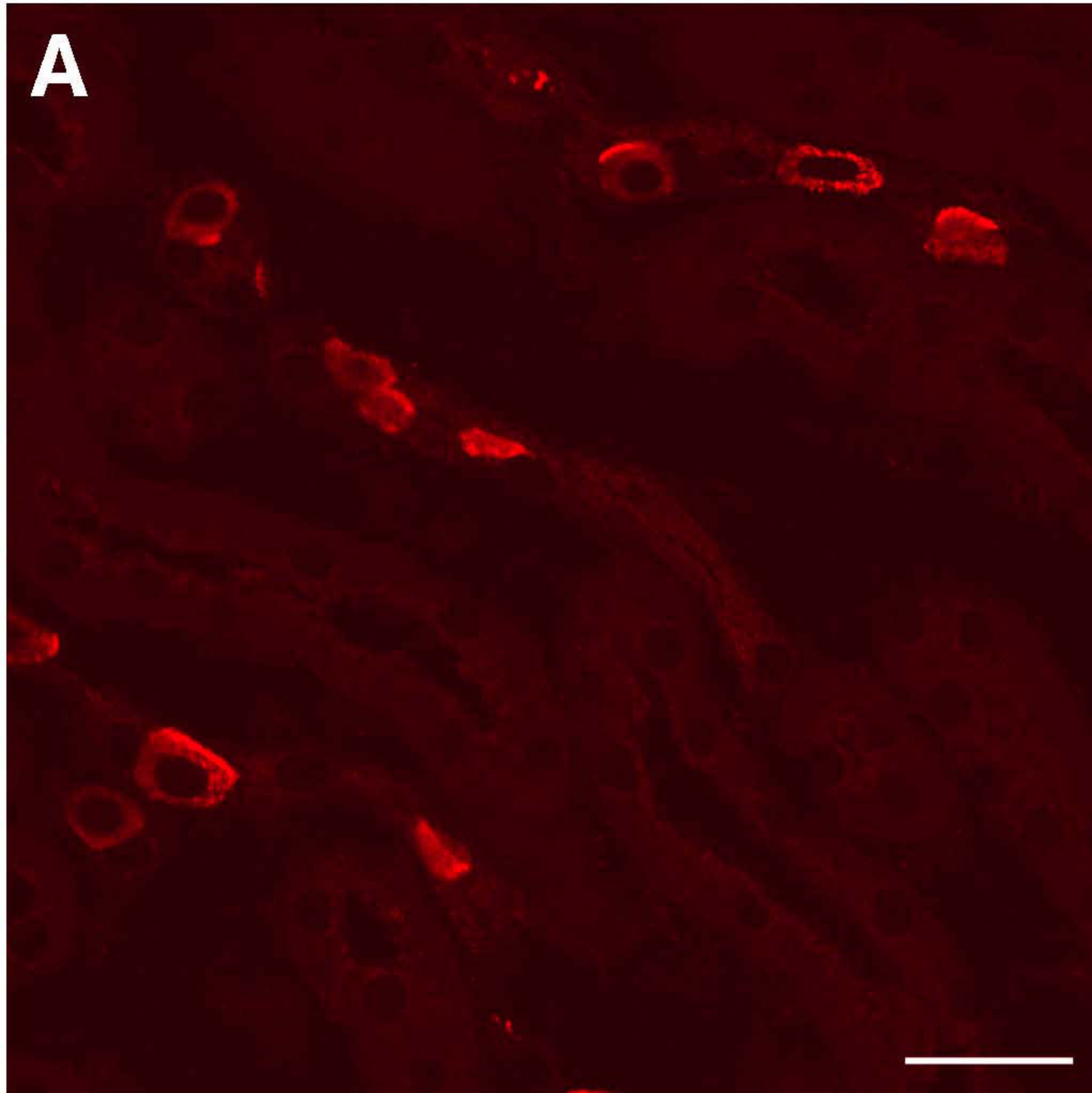
Urine osmolality, mmol/kg	2300 ± 616 (3)	2320 ± 367 (4)	0.9772	0.9509	0.5003
Water intake, ml/g BW	0.36 ± 0.07 (4)	0.33 ± 0.03 (4)	0.7304	0.0111 (*)	0.0002 (***)
NaHCO ₃ load, mmol/g BW	0.100 ± 0.019 (4)	0.093 ± 0.008 (4)	0.7304	N/A	N/A

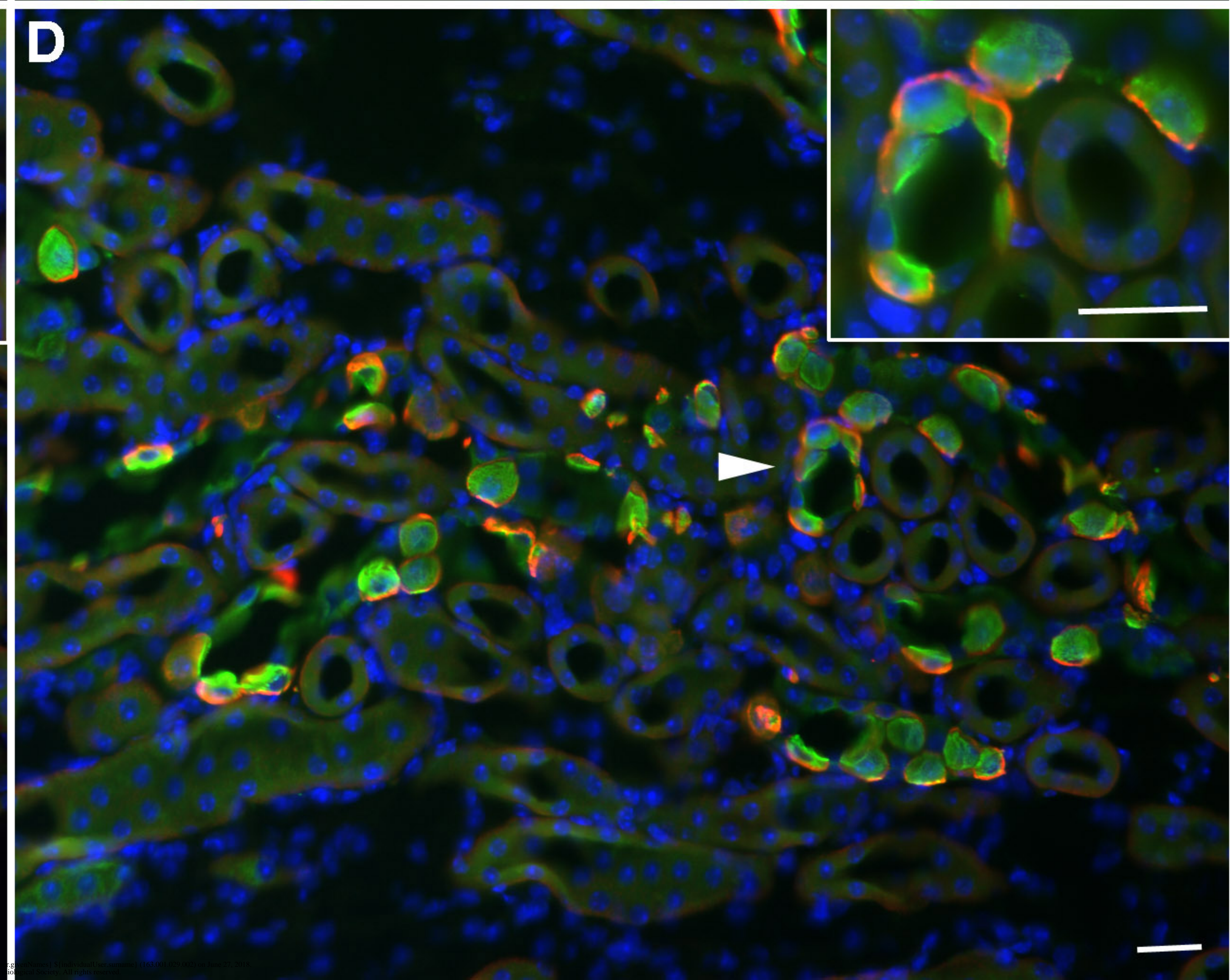
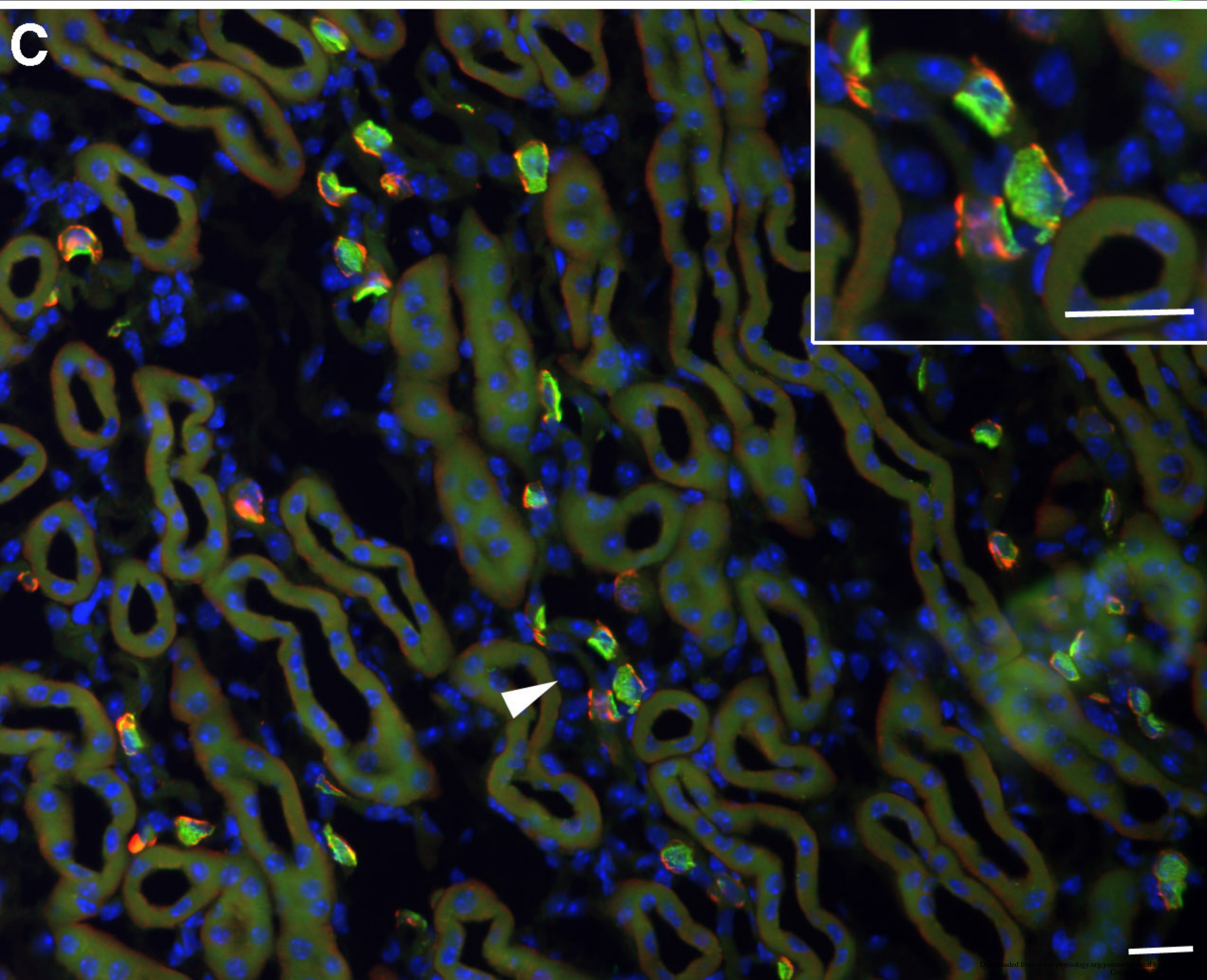
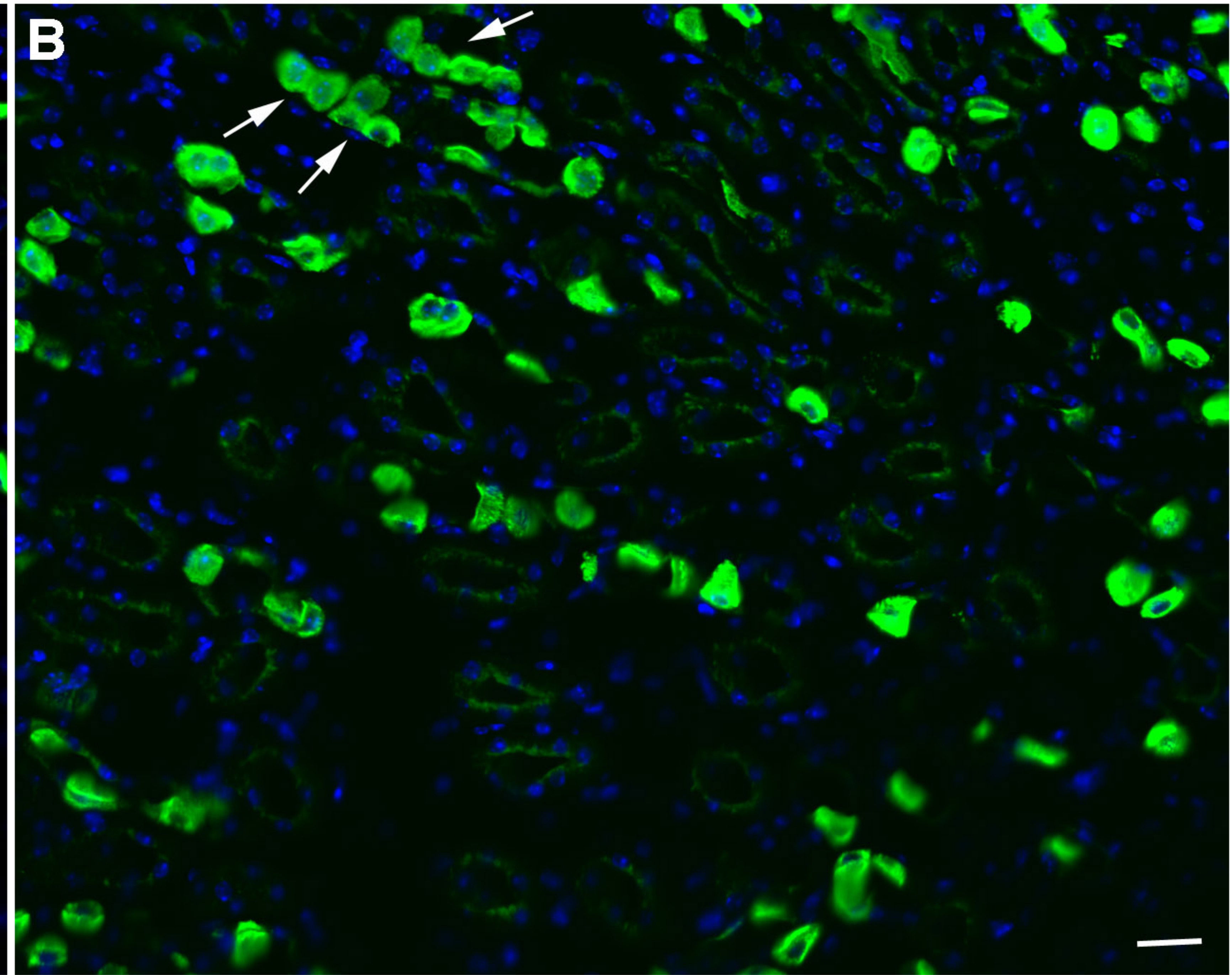
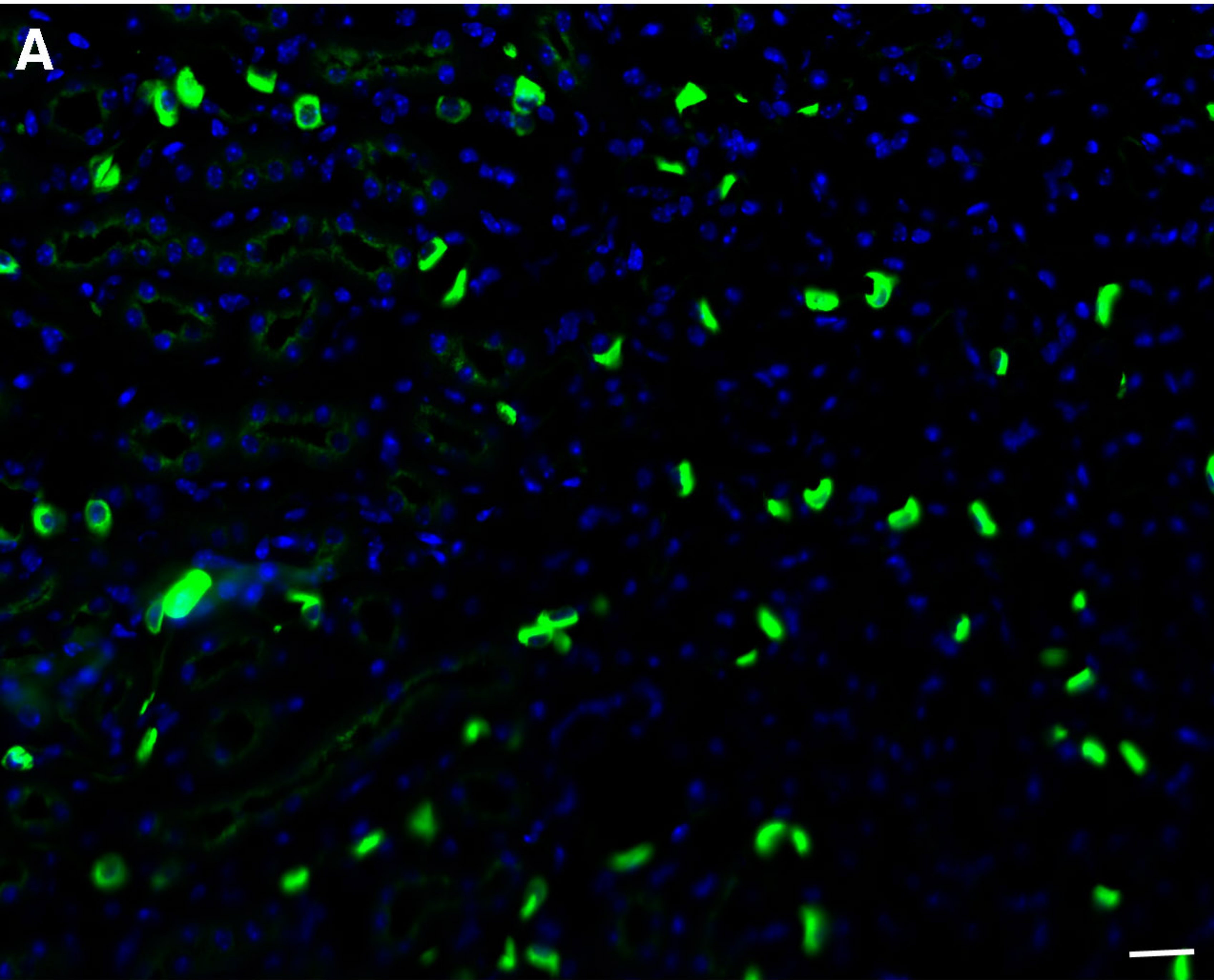
All values are means ± SEM. Numbers of animals are in parentheses. * is for p-value < 0.05, ** is for p-value < 0.01, *** is for p-value < 0.001, **** is for p-value < 0.0001; t-test. N/A = not applicable.

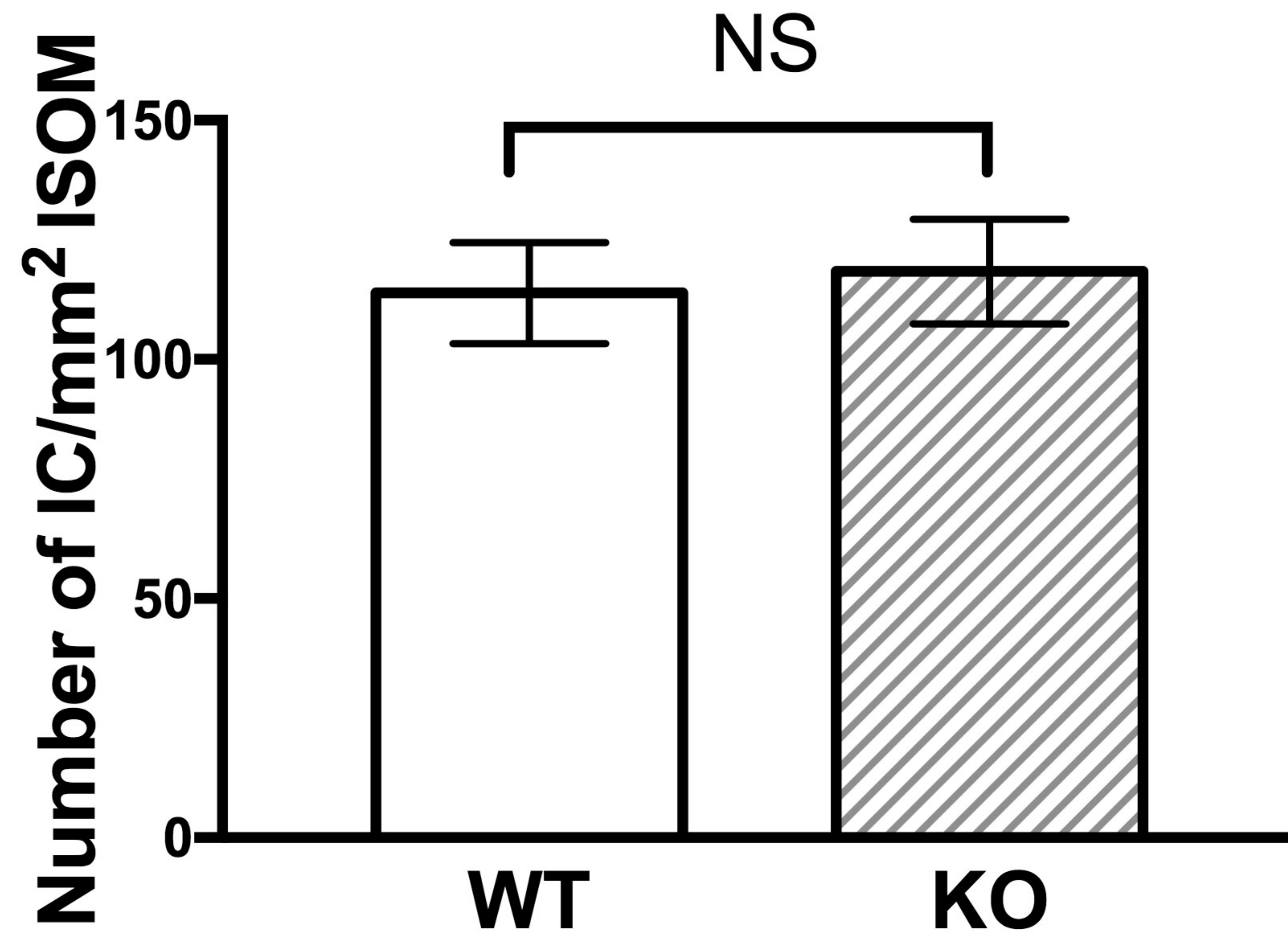




A**B**





A**B**